Computational Materials Science 199 (2021) 110720

Contents lists available at ScienceDirect

Computational Materials Science

journal homepage: www.elsevier.com/locate/commatsci

A review of computational studies of bottlebrush polymers

Esmat Mohammadi [a], Soumil Y. Joshi [b], Sanket A. Deshmukh [b,*]

[a] Department of Chemical Engineering, University of Guilan, Rasht, Guilan, Iran
[b] Department of Chemical Engineering, Virginia Tech, Blacksburg, VA 24061, United States

ARTICLE INFO

Keywords:
Theory and Simulations
Bottlebrush polymers
Polyelectrolytes
Stimuli-responsive polymers
Self-assembly

ABSTRACT

Bottlebrush polymers (BBPs) are a class of grafted polymers, which have attracted much attention due to their wide range of novel applications. The properties of these grafted polymers can be easily tuned by changing architectural parameters like grafting density and the degree of polymerization of the side chains and backbone. Moreover, environmental factors like solvent quality, temperature, pH, etc. can tremendously affect the BBPs' conformations and thus their properties. Consequently, a considerable number of experimental and computational studies have been conducted to investigate the conformations of BBPs under various circumstances. Computational approaches including particle-based and field-theory-based methods have been widely implemented in recent decades to study BBPs. This paper reviews articles that investigate BBPs in solution, on surface and in the melt states using computational methods. In addition to neutral BBPs, properties of bottlebrush polyelectrolytes, stimuli-responsive polymers and the factors affecting their conformations are discussed. Finally, we discuss the computational studies on self-assembly of BBPs and the factors determining resulting morphologies of the self-assembled structures.

1. Introduction

Inspired by the shape and design of an incredibly complex group of biomolecules known as proteoglycans (Fig. 1), bottlebrush polymers (BBPs) are branched polymers consisting of polymeric side chains anchored to a linear backbone [1]. These structures, also called molecular brushes or cylindrical polymer brushes [2–4] have various architectures [5]. These can be categorized based on their structural specifications like the orientation of their backbone and side chains as well as their grafting densities as depicted in Fig. 2. BBPs have attracted much attention because of their potential applications in lubrication [6], drug delivery [7], sensing [8], photonics [9], interfacial modifications [10], and shape-memory materials [11]. For targeted applications, changing the structural and/or environmental parameters such as the solvent [12,13], temperature [14–17], pH [18–20], salt concentration [19], etc., makes it possible to tune the BBP conformations and their properties. A large number of studies have focused on designing and investigating BBPs through different experimental or computational approaches in order to understand their conformational properties under various conditions like in solutions, on surfaces, and in melt states [21–26]. Moreover, both computational and experimental approaches have been integrated to engineer particular BBP geometries in order to obtain the macromolecules with desired specifications [27].

Due to limitations in resolution, it is difficult to understand the relationship between microscopic conformational details and the reasoning behind the polymer's properties at the molecular-level and at short time-scales (below 10s of nanoseconds) experimentally, which makes computational approaches very attractive [28]. In the case of BBPs, these microscopic details usually include the grafting density, backbone and side chain lengths, etc. The application of theoretical or analytical methods to study these microscopic details and predict the molecular-level behavior of BBPs can also be challenging [29,30]. Hence, computational approaches have garnered a lot of attention due to the sophisticated algorithms used for numerical calculations, significant improvements in computational capabilities, and the current state-of-the-art models, which can accurately predict the structure and properties of BBPs at the molecular-level [31–33]. Indeed, it has been demonstrated that molecular simulations are advantageous in predicting the molecular structure and behavior of BBPs [34–36], as well as for validating results gained from theoretical predictions [37]. Scaling theories, on the other hand, are frequently used to map the properties of polymers onto simple relations in order to link a selection of microscopic details to a set of general features [38]. To the best of our knowledge, most of the review papers presented on BBPs over the last decade,

* Corresponding author.
E-mail address: sanketad@vt.edu (S.A. Deshmukh).

https://doi.org/10.1016/j.commatsci.2021.110720
Received 2 February 2021; Received in revised form 8 July 2021; Accepted 9 July 2021
Available online 2 August 2021
0927-0256/Published by Elsevier B.V.

review the results obtained through experimental procedures with little discussion about relevant computational studies [39–41]. Thus, particularly reviewing these computational studies used to explore BBP conformational properties seems of essence for the current scientific landscape.

In this review paper, we will first introduce the theoretical modeling and simulation approaches including particle-based and field-theory-based methods used to study BBPs. Next, we focus on the studies that have used these computational methods to investigate the behavior of BBPs in solutions, on surfaces and in melt states. In this regard, we mainly concentrate on investigating the effect of degree of polymerization of side chains and backbone, and grafting density on the molecular conformation. In Sections 4 and 5, we provide a review of simulation studies on stimuli-responsive BBPs and bottlebrush polyelectrolytes, respectively. This is followed by a review of self-assembly simulations of BBPs in Section 6. Finally, in Section 7 we provide a summary of this review, known drawbacks of existing methods and potential areas of improvements for studying BBPs by integrating existing methods with machine learning approaches.

2. Theoretical modeling and simulation methods

Particle-based and field-theory-based simulations have been widely used to study structural, physical, rheological and thermodynamic properties of BBPs at different length- and time-scales [35,43,44]. Here, we introduce some of these simulation methods that are regularly used to model BBPs and discuss their advantages and limitations in simulating BBPs. Molecular dynamics (MD), Brownian dynamics (BD), dissipative particle dynamics (DPD) and Monte Carlo (MC) simulations are classified as the particle-based techniques. These methods, over the years, have proven to be advantageous in gaining molecular insights and predicting the equilibrium properties of polymeric systems. However, these methods are computationally expensive to simulate bigger systems with large length-scales, particularly, when it comes to calculating long-range interactions using the Ewald summation method [45–47]. On the other hand, field-theory-based approaches have been used for approximate analytical calculations on a variety of complex fluid systems including polymer solutions, melts, blends, and copolymers [48]. The ease of capturing long range interactions in simulations of BBPs with immense sizes is regarded as one of the advantages of these methods, drastically decreasing their computational demand as compared to the particle-based techniques [49,50]. Moreover, the mechanical properties of BBPs, like bending modulus, can be directly obtained from these models using their partition functions as opposed to particle-based simulations, where properties have to be indirectly calculated by analyzing the shape of BBPs [51]. While field-theory-based simulations are computationally cheaper than particle-based methods for dense systems of long polymers, where a coarse computational grid suffices to capture mesoscopic structure, they fall short when fewer molecules have to be described on microscopic scales or when atomistic chemical details are required [52,53]. Their universality is also limited to systems where the assumptions of the standard Gaussian chain model (GCM) are satisfied [54]. In the section below we will briefly introduce the most commonly used particle-based and field-theory-based simulation techniques to study BBPs.

2.1. Particle-based simulations

2.1.1. Molecular dynamics simulations

Molecular dynamics (MD) simulations is one of the most prevalent particle-based methods, which is widely used to gain insight into the structure and dynamic evolution of biomolecules [55,56], proteins [57,58], and polymers [59–62]. This method generates a trajectory of the studied system by iteratively solving Newton's equations of motion, based on a set of interaction potentials, also known as force-field parameters [63–65]. In general, these interactions can be divided as bonded and nonbonded interactions (Eq. (1)). The bonded interactions, most commonly represented by a harmonic potential, can be calculated by the summation of bond, angle, dihedral and improper potential functions (Eq. (2)). The nonbonded interactions can be represented through electrostatic and Van der Waals energies (Eq. (3)). In Eq. (2), the parameters b, θ, φ, and ϑ represent bond length, bond angle, dihedral angle and improper angle between the particles, respectively, whereas, b_0, θ_0, φ_0, and ϑ_0 are the equilibrium values for these parameters. Since

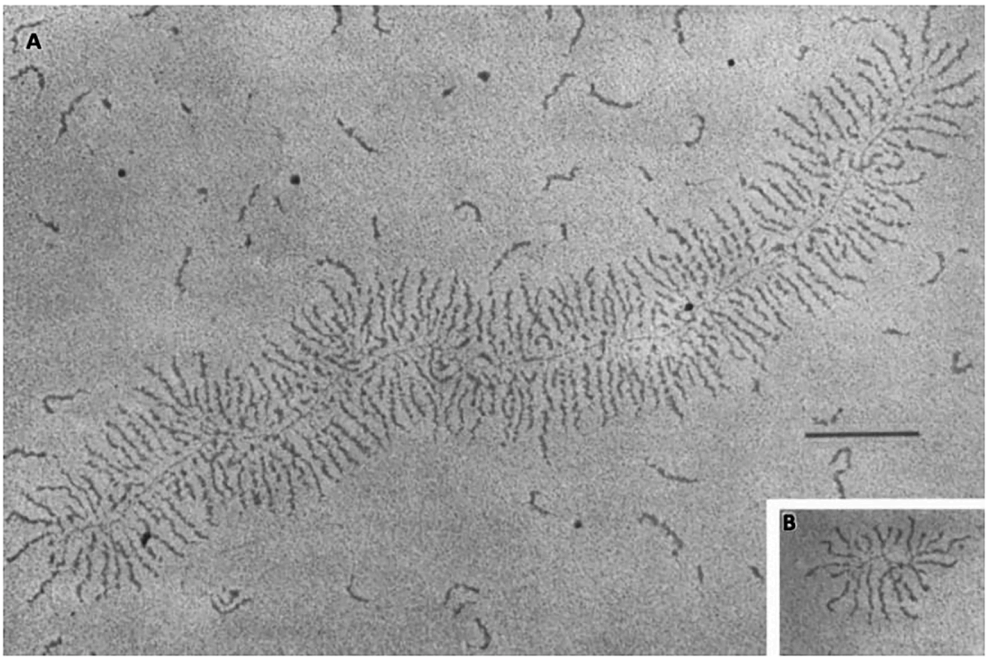

Fig. 1. Electron micrographs of bovine articular cartilage proteoglycans. A) A large proteoglycan aggregate from a calf consists of a central hyaluronic acid filament and multiple aggregated monomers surrounded by nonaggregated monomers. B) A typical steer proteoglycan aggregate. *Reprinted with kind permission of Wiley publication and* [42]. *Copyright (1985) Orthopaedic Research Society.*

particles are assumed to be attached to one another *via* virtual springs, k_b, k-$_\theta$, k_φ, and k_ϑ are often regarded as spring force constants, and are used to calculate the various bonded interactions. The two terms in Eq. (3), which relate to nonbonded interactions consider the partial charges on atoms as q-$_i$ and q_j while r_{ij} is the distance between particles i and j. ϵ is the Lennard-Jones well depth and σ is the distance at which the Lennard-Jones potential has the minimum value. The forces between the particles are calculated as the negative gradient of the potential energy and are finally used in Newton's equation of motion (Eq. (4)) to obtain the trajectory of each particle in the system. In this regard, detailed discussion is provided in these important textbooks [66–68].

$$U = U_{bonded} + U_{nonbonded} \tag{1}$$

$$U_{bonded} = \sum_{bonds} k_b(b-b_0)^2 + \sum_{angles} k_\theta(\theta-\theta_0)^2 + \sum_{dihedrals} \frac{k_\varphi}{2}(1 + cos(n\varphi-\varphi_0)) + \sum_{impropers} k_\vartheta(\vartheta-\vartheta_0)^2 \tag{2}$$

$$U_{nonbonded} = \sum_{i=1}^{n-1}\sum_{j>i}^{n} \frac{q_i q_j}{4\Pi\epsilon r_{ij}} + \sum_{i=1}^{n-1}\sum_{j>i}^{n} 4\epsilon\left[\left(\frac{\sigma}{r_{ij}}\right)^{12} - \left(\frac{\sigma}{r_{ij}}\right)^{6}\right] \tag{3}$$

$$m_i\frac{d^2r_i(t)}{dt^2} = F_i(t) \tag{4}$$

All-atom (AA) and coarse-grained (CG) schemes are generally used to represent molecules in MD simulations, based on whether the questions that are being addressed need the atomic-level or molecular-level description of molecules. Investigating large systems such as solvated bottlebrushes at the atomic-level can be computationally very expensive. Hence, BBP simulations are often performed using CG models to study the overall conformations of these BBPs without considerable computational expenditure. CG models exclude the minute interatomic calculations that may not be of significant interest when studying such complex structures [16]. CG MD simulations have been employed to study individual BBPs in melt state, on surfaces, as well as in the presence and absence of explicit solvents [35,69–71]. However, performing self-assembly simulations of BBPs in the presence of explicit solvents, even with CG models, still remains a challenge due to their larger length- (several million atoms) and time- (several microseconds) scales.

2.1.2. Brownian dynamics simulations

In Brownian dynamics (BD) simulations, the force that governs the equation of motion is calculated by Langevin equation (Eq. (5)) [72]. F_{ij} is the conservative force applied on particle i by particle j, $P_i(t)$ is the momentum of particle i, γ and σ are constants, defined for the system, and $\xi_i(t)$ is Gaussian random noise.

$$m_i\frac{d^2r_i(t)}{dt^2} = \sum F_{ij}{}^{c}(t) - \gamma P_i(t) + \sigma\xi_i(t) \tag{5}$$

The effect of solvent on polymer is considered by using the dissipative and random forces that are presented in Eq. (5) with $\gamma P_i(t)$ and $\sigma\xi_i(t)$, respectively. Since BD uses the implicit solvent particles rather than the explicit solvent, this method is more computationally efficient to simulate BBPs up to several microseconds. Thus, one of the advantages of BD simulations is the possibility of using this method for simulating multicomponent systems with considerably different time scales for the individual components in the system [73,74]. To illustrate the point, consider a solution consisting of polymers and solvent, in which the solvent molecules have faster motions and need a shorter time step to be simulated, whereas the motion of solute particles can be predicted in larger time steps due to their larger sizes [72]. In such systems, as the solvent is implicitly modeled using BD, larger time steps corresponding to the solute can be utilized.

The main drawback of BD simulations is that the energy and momentum may not be conserved. As a result, BD simulations do not properly take the hydrodynamic interactions into account [72,73,75], as they are typically applied through momentum exchange between solvent and polymer molecules [76]. However, several groups have employed the Rotne-Prager-Yamakawa approximate diffusion tensor to include the hydrodynamic interactions in BD simulations [77–85]. Detailed information on the BD methods for polymer simulations can be found in various articles and books [77,78,86,87]. BD simulations have been shown to be efficient in predicting the self-assembled BBP/surfactant complexes [88], and in combination with Monte Carlo, BD can predict the equilibrium conformations of BBPs in dilute solutions [36,89]. However, BD is rarely employed for simulating BBPs in other

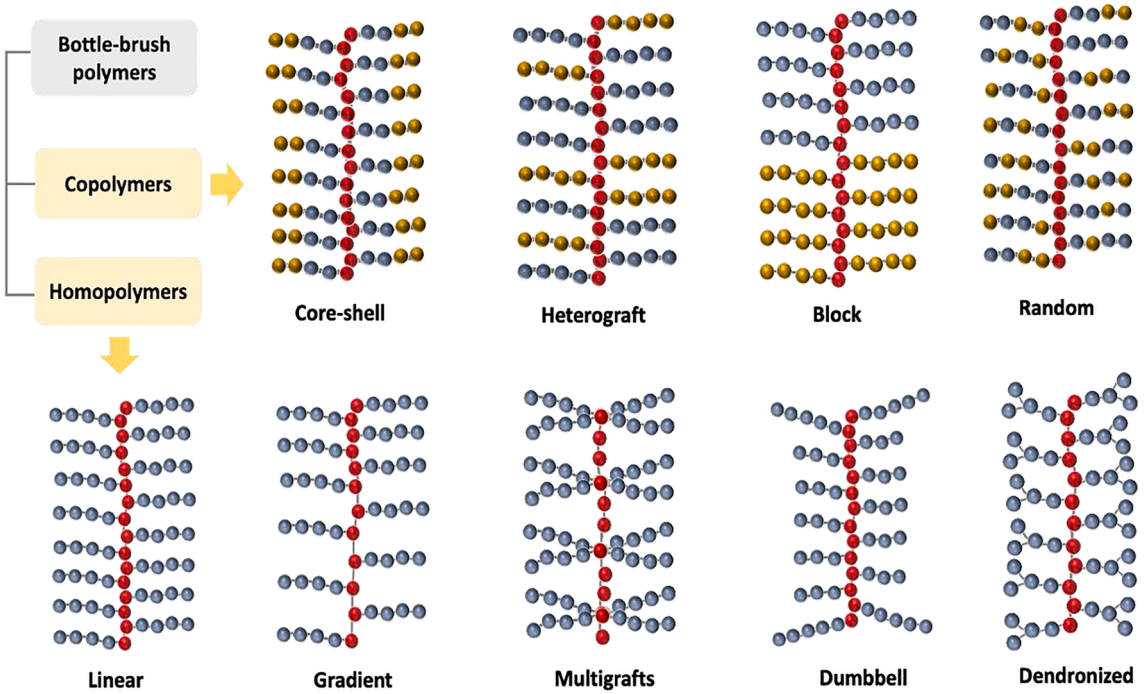

Fig. 2. Various branching topologies of bottlebrush polymers.

states like melts, in thin films and grafted on surfaces.

2.1.3. Dissipative particle dynamics simulations

Dissipative particle dynamics (DPD) simulations, first presented by Hoogerbrugge and Koelman [90] have proven to be useful in simulating large systems of Newtonian or non-Newtonian fluids involving melts and blends of polymers [91–97]. In the DPD method, each particle represents a group of molecules, drastically decreasing the number of particles in the system as compared to MD and BD simulations [72]. Newton's equation of motion is used to predict the displacement of these particles, which is similar to MD simulations [98]. The overall force exerted on a particle is a combination of three forces including conservative, dissipative and random forces that are represented by F_{ij}^{C}, F_{ij}^{D} and F_{ij}^{R} respectively, in Eqs. (7)–(9) [94]. Eq. (7) is valid for the distances less than the cut-off distance, and term a_{ij} is the maximum possible repulsion between the particles, r_c is the cut-off distance, and $\hat{r}_{ij}$ is a unit vector. In Eqs. (8) and (9), ω^D and ω^R are the weight functions for the dissipative and random forces [99], γ is the friction coefficient, σ is the noise amplitude and Θ_{ij} is a noise term with Gaussian distribution. Further details on this method can be found in literature [98–101].

$$F_{ij} = \sum F_{ij}{}^{C} + F_{ij}{}^{D} + F_{ij}{}^{R} \tag{6}$$

$$F_{ij}{}^{C} = a_{ij}\left(1 - \frac{r_{ij}}{r_c}\right)\hat{r}_{ij} \tag{7}$$

$$F_{ij}{}^{D} = -\gamma\omega^{D}(r_{ij})\left(\hat{r}_{ij}.v_{ij}\right)\hat{r}_{ij} \tag{8}$$

$$F_{ij}{}^{R} = \sigma\omega^{R}(r_{ij})\Theta_{ij}\hat{r}_{ij} \tag{9}$$

Another advantage of DPD simulations over MD simulations, except the fewer number of particles in the system, is that the conservative force exerted on particles decreases linearly with increasing r_{ij} [72]. As a consequence, it allows adopting larger time steps to perform simulations of polymer systems consisting of BBPs for longer time-scales [73,75]. Furthermore, similar to MD simulations, solvent molecules can be simulated in the system explicitly through DPD simulations, which is not the same in BD [72,73]. Although the existence of dissipative and random forces leads to diminishing energy conservation of the system, the momentum is conserved in DPD simulations, which creates a context to consider the hydrodynamic interactions that can be essential in the self-assembly process of BBPs in solutions [75]. All these advantages make DPD simulations appealing for simulating large systems consisting of BBPs. Indeed, DPD simulations are widely used to investigate the self-assembly of BBPs leading to the formation of microstructures in solutions [102–104]. They have also been employed for simulating the self-assembly of amphiphilic comb-like graft copolymers with pH-sensitive side chains where pH variation, controlled by changing solvent quality, is a determining factor in the formation of various morphological conformations [105]. Moreover, DPD has also been shown to be advantageous to study BBPs in other states like thin films [106].

2.1.4. Monte Carlo simulations

Monte Carlo (MC) simulations work based on a stochastic approach using random numbers to predict the positions of the particles [72,75,107]. This dynamic process can be summarized in three steps. First, the initial positions of the particles are assumed to be $\{r_1, r_2..., r_i, r_n\}$ and the related potentials are specified as $u = \{u\text{-}_1, u\text{-}_2..., u\text{-}_i, u_n\}$. Then, changing the position of the particle i from r_i to $r_i^{'}$ contributes to the overall positions of $\{r_1, r_2..., r_i^{'}, r_n\}$, which leads to a variation in potential ascertained as $u^{'} = \{u\text{-}_1, u\text{-}_2..., u\text{-}_i^{'}, u_n\}$. If the overall potential change in the system $(\Delta U = u\text{-}u^{'})$ is negative, the new positions seem reasonable because the system has evolved to a lower state of energy. If $\Delta U > 0$, there is a condition that needs to be addressed which is $\exp(-\Delta U/k_BT) \geq \alpha$, and α is a random number in a range of zero to one. Otherwise, the original position of the particle is assumed to be the new position. This procedure is repeated until the position of all particles are updated. Further discussion on the details of this method is accessible in literature [108–110].

Although the calculation of the forces in MC is neglected, it is one of the essential steps in calculating the trajectory of the particles in MD [75]. MC is useful for analyzing the statistical physics of systems which cannot be analyzed through MD simulations. In addition, the investigation of the dynamics of the system by MC is derived from mathematical approximation rather than physical laws of dynamics as observed in MD [75]. Thus MC can be used just for prediction of equilibrium properties of the system, while MD provides information on both equilibrium and non-equilibrium properties of the system [72]. Even though the differences between MD and MC simulations have been studied already, it seems that comparison between MC and other methods has not been addressed widely in the literature.

MC simulations have been mainly used for simulating BBPs adsorbed on surfaces and in thin films, as well as in solutions [111–115]. One of the challenges mentioned in the literature for BBP simulations using particle-based methods is attributed to the very long simulation time in order to calculate equilibrium configurational properties [116]. These properties should ideally be calculated from a subset of configurations from a large number of molecules, after reaching the equilibrium state in a very long simulation run [116]. In order to reduce the computational cost, the use of single BBPs in a periodic boundary condition, instead of a large number of BBPs, has been reported [116].

2.2. Field-theory-based simulations

First proposed by Edwards in 1965 [117], a different strategy to tackle the shortcomings of particle-based methods is to replace the coordinates and momenta of particles (polymer segments) with collective variables, or fields - which forms the basis of field-theory-based simulations. A field-theory-based simulation is a numerical strategy suitable for simulating long-range interactions, as well as studying equilibrium properties of many-particle systems like complex self-assemblies of BBPs, within the framework of a statistical field theory [53]. By doing so, the complicated atomistic structure of the monomers becomes irrelevant on the molecular scale, and in turn, the equilibrium phase behavior becomes universal [54]. The Gaussian chain model (GCM), for example, is a minimal model whereby a polymer melt is treated as an incompressible system of elastic threads interacting by contact forces, and has emerged as the standard model for block polymer phase behavior [118]. Other important field-theory-based methods including the self-consistent field theory (SCFT) and the field-theoretic polymer simulation (FTPS) are discussed in detail, later in this section. But first, we briefly introduce the unified theoretical framework underlying these methods. More details on this can be found in references [50].

For an incompressible AB diblock copolymer, with polymerization index N and the block composition of fA in a volume V, the canonical ensemble partition function can be written as:

$$Z = \int DW_{+} \int DW_{-}\ exp(-H[W_{+}, W_{-}]) \tag{10}$$

Where DW_{+} and DW_{-} are fluctuating chemical potential fields introduced through HS transformation, DW is a functional integral over the chemical potential fields, and $H[W_{+}, W_{-}]$ is the effective field-based Hamiltonian [50,75]. General strategies to evaluate the field-theoretic model by solving this Hamiltonian include (i) using analytical approximations to simplify the theory and then applying analytical or numerical methods to extract information from the simplified theory, and (ii) generating the numerical approximations to the exact field theory.

2.2.1. Self-consistent field theory (SCFT)

Used since as early as the 1960s [117,119,120], SCFT utilizes the first of the aforementioned strategies to evaluate polymer field-theory-

based models. SCFT applies the mean-field approximation where the saddle point of the Hamiltonian dominates the partition function, and the field fluctuations around the saddle point are ignored [119]. SCFT calculations are way less expensive than competing particle-based simulation methods. However, SCFT is efficient while investigating the thermodynamic properties of polymer systems in which the mean-field approximation is valid [75]. The accuracy of SCFT is greatly affected by the dimensionless chain concentration C. For low value of C, such as the polymer solutions in dilute or semi-dilute regimes, or for the study of smaller polyelectrolytes, the functional integral that defines the configuration partition function of the field-theoretic model does not solely depend on the saddle point configuration and mean-field methods may not be highly accurate [53,54]. These limitations can be tackled by implementing the second strategy for evaluating polymer models through the use of field-theoretic simulations (FTS) [75]. SCFT has been utilized to study the interfacial behavior of BBP copolymers [121], as well as to investigate the interactions between polyelectrolyte BBPs and charged surfaces [30]. Besides, SCFT has also been used to analyze the self-assemblies of a variety of BBP systems [122].

2.2.2. Field-theoretic simulations (FTS)

While conceptually similar to SCFT, the aim of FTS is to numerically sample the statistically important field configurations of the full theory, rather than just the saddle point configuration [54,123]. In doing so, this method obtains accurate fluctuation corrections to SCFT, by simulating the Hamiltonian, $H[W_+, W_-]$[54]. However, standard simulation techniques for integrating over the fields are not applicable. This is because the pressure field, W_+, is imaginary, which leads to a complex-valued Hamiltonian, and thus, a Boltzmann weight is not positive definite. To tackle this, two strategies have been utilized - (i) the steepest descent technique (STD-FTS), which shifts the integration to follow a constant-phase path through the saddle points of SCFT, and (ii) the more efficient complex Langevin simulations (CL-FTS), whereby both fields sample the entire complex plane [54,123]. One of the main advantages of the FTS approach is its incredible versatility as well as their lower computational cost when the systems are dense, polymers are long, and length scale is large [53]. Being a fairly recent method, BBP specific studies employing FTS are limited. FTS has been used to study the effect of grafting density on the order–disorder transition (ODT) of BBP copolymers as well as the phase transition behavior in BBP homopolymer melts [49,124].

3. Molecular conformation of bottlebrush polymers in melts, on surfaces and in solutions

In the following sections, we review the computational studies exploring the effects of structural and environmental factors on BBP conformations and their properties in melt state, solutions, films as well as on surfaces.

3.1. Molecular conformations in melts

BBPs in melts exhibit high elasticity [125,126], making them appealing candidates for applications including electroactuation [127], adhesive coatings [128], implants [129], and composites [130]. Hence, BBPs have been investigated in melt state to tailor these properties for certain aimed applications. However, despite considerable developments in this area, there are still difficulties associated with the existing experimental procedures [69], facilitating the emergence of computational research. Over the years, particle-based simulations have been widely used to demonstrate the relevance between architectural parameters and thermodynamic, physical, rheological, conformational and structural properties of BBPs at the molecular-level [69,131–133], while field-theory-based models have been employed to investigate their phase behavior in melt state [49,124].

Liang *et al.* employed CG MD simulations using a bead-spring model with scaling analysis to clarify the regimes and sub regimes in which grafted polymers appeared in melt state [134]. A crowding parameter ($\phi \approx [\nu/(lb)^{3/2}][(n_{sc}/n_g + 1)/n_{sc}^{1/2}]$) was defined, based on architectural parameters like the degree of polymerization of the side chains (n_{sc}), the number of backbone bonds between the grafted side chains (n_g), as well as the chemical composition of the monomers including bond length (l), Kuhn length (b) and excluded volume of the monomers (v). It was shown that for $\phi < 1$, grafted side chains were sparse around the backbone and were categorized as comb-like macromolecules, while for $\phi > 1$ densely grafted BBPs were formed in melt. BBPs, with higher grafting densities, were observed to demonstrate different interpenetration behavior as a result of changing the crowding parameter. Specifically, the interpenetration of side chains and backbones of neighboring BBPs was less than that of comb-like macromolecules because of the higher steric repulsion between the chains of BBPs. Moreover, they studied the effective Kuhn length and mean-square end-to-end distance of these branched macromolecules to show that increasing the crowding parameter resulted in increasing Kuhn length and end-to-end distance. They attributed this behavior to the stiffening of the backbone due to increased interactions between the side chains. In order for the melt density to be constant at high grafting densities, BBPs possessed different conformations with stretched backbones or side chains, resulting in three sub regimes as shown in Fig. 3A [134]. In another study, they further studied the crossover from comb-like macromolecules to BBPs in melt state using MD simulations, by investigating their packing number (P_e), which indicated the number of polymers needed for the side chains to entangle in a surrounded tube [135]. They found that this parameter was related to the ratio between the size of side chains and the distance between the neighboring grafted chains, and thus dependent on the molecular architecture. The study indicated that at first when this ratio increased, the packing number decreased. However, a further increase led to an increase in the packing number, demonstrating that a transition from comb to BBP could be observed when the size of side chains and grafting density increased [135].

Chremos and Douglas performed MD simulations on BBPs with various side chain lengths, grafting densities and backbone lengths in melt condition to delineate the effect of architectural parameters on the overall shape of BBPs in melt [69]. The results revealed that BBPs with backbones shorter than the grafted side chains resulted in the formation of ellipsoidal shapes. As the backbone lengths became comparable to the side chain lengths, the overall structure formed a spherically symmetric shape. Whereas, for the BBPs with longer backbones compared to the side chains, the molecular brushes adopted overall anisotropic structures. These observations were further probed by calculating three spatial correlations between the polymer segments - (i) Overall structure factor, (ii) Backbone structure factor and (iii) Bottlebrush and backbone form factor [69]. In another study by Paturej *et al.*, the analysis of MD trajectories revealed that increasing grafting density, defined as the number of side chains per backbone monomer, as well as increasing the degree of polymerization of the side chains caused the backbone to be more extended due to the steric repulsion between side chains. It also led to increased intra- and intermolecular interactions between monomers contributing to less overlap between side chains of the surrounding BBPs [136]. It was observed that for intermediate grafting densities ($z \leq 2$), BBPs resembled flexible filaments. While for higher grafting densities ($z > 3$) and short backbones ($N_{bb} \leq 50$), rigid rod-like structures were observed because of the increased persistence length of the backbone as a result of increasing grafting density [136]. A field-theory-based study on bottlebrush copolymers by Spencer and Matsen investigated the effect of grafting density and the spacing between grafted chains on order–disorder transition (ODT) of BBPs with diblock side chains [49]. The interactions between different blocks were controlled using the Flory-Huggins parameter, χ. ODT was located from parallel tempering (PT), using an order parameter, $\langle \Psi \rangle$. They showed that reducing the spacing between grafted chains, at a fixed grafting density, caused BBPs to behave like star block copolymers and enhanced the ordering of BBPs.

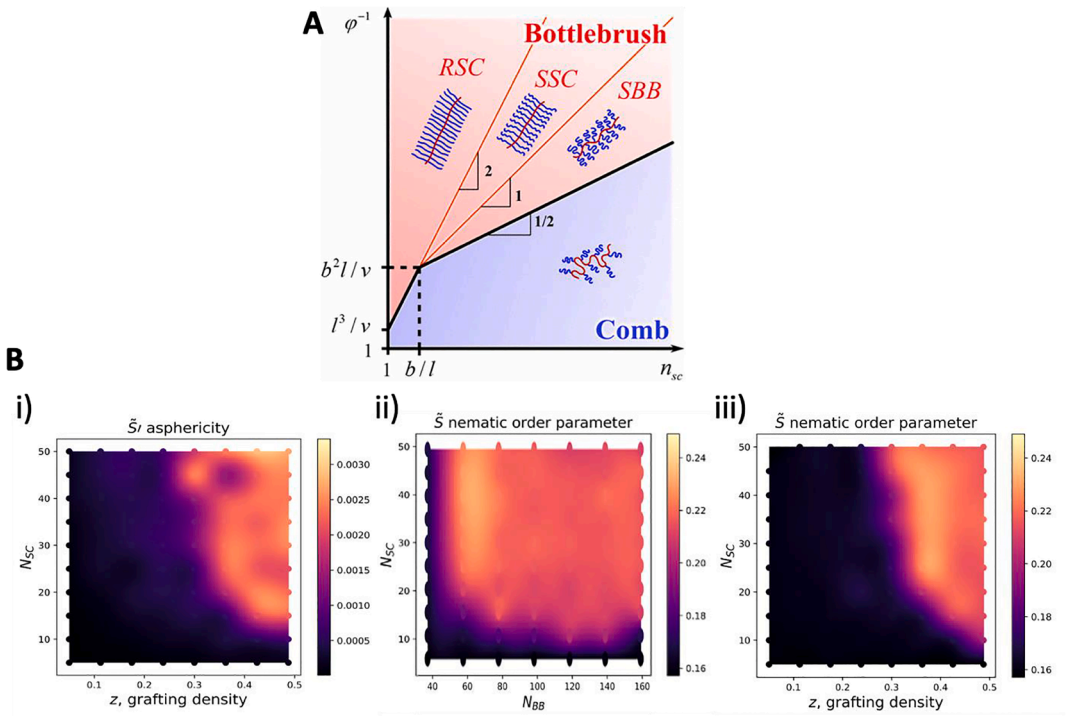

Fig. 3. A) Diagram of states of graft polymers in a melt. SBB – stretched backbone regime, SSC – stretched side chain regime, and RSC – rod-like side chain regime. Logarithmic scales. *Reprinted with permission from* [134]. *Copyright (2017) American Chemical Society.* B) (i) The nematic order parameter derived from S'. In particular, the asphericity increases in the nematic phase. (ii) The nematic order parameter as a function of backbone length and length of side chains for a fixed grafting density $z = 0.4875$ (corresponding to a grafting spacing $d = 2$). Subspace averaging was employed with $c = 4\ l$ (iii) The nematic order parameter derived from S as a function of grafting density and length of side arms for a fixed backbone length, $N_{BB} = 100$. A clear contrast is seen between two regions, which we identify as isotropic (blue) and nematic (yellow). The nematic order parameter is averaged over subcells of size $c = 4\ l$. We also examined $c = 2\ l$ and $8\ l$ (not shown) with no significant differences evident on the boundary of the nematic phase transition, but small quantitative differences in the intensity within the bounded area. *Reprinted from* [124], *with the permission of AIP Publishing.* (For interpretation of the references to color in this figure legend, the reader is referred to the web version of this article.)

In this study, the lamellar phase was considered as an ordered structure of BBPs. Consequently, decreasing the spacing between the grafted side chains resulted in the decrease of order–disorder transition, which was apparent in increasing the order–disorder temperature. In contrast, increasing the spacing between side chains caused BBPs to behave more like diblock copolymers, leading to increasing the transition from an ordered to disordered structure. This was attributed to the suppressed segregation of polymers when the spacing between side chains was higher, caused by the fluctuation effects. However, fluctuation effects did not affect densely grafted polymer chains and their ODT decreased [49].

There are few studies investigating the effect of grafting density and side chain length on the structural transition of BBPs to a nematic phase (parallel orientation of molecules relative to their long axis). For BBPs in melt state, using field-theory simulations, Panagiotou *et al.* showed a phase transition, from isotropic (disordered orientation of molecules) [137,138] to nematic phases [139] for relatively wide ranges of grafting densities, and side chain and backbone lengths [124]. It was observed that as side chain length and grafting density was increased, BBPs possessed nematic structures as a result of field fluctuations, resulting in higher asphericity [140–142] values in the nematic zone (Fig. 3B). Thus, it demonstrates the importance of architectural parameters on the orientation and conformation of BBPs [124]. Borodinov *et al.* integrated CG MD simulation with an experimental approach to study the molecular arrangement of BBPs in a thin film [143]. Their experimental results showed a molecular reorganization of BBPs from a random organization to nematic structure. They reported that when BBP film on a surface was annealed, the system reached an equilibrium state and the random orientation of BBP backbones rearranged to a nematic structure. This observation was attributed to the steric hindrance favoring an ordered packing of BBPs. Indeed, they believed that the BBPs used in their study were rigid enough to form the liquid-crystalline structure. Additionally, they employed CG MD simulations and the results showed the realignment of the BBPs in the film to have an ordered packing. This molecular reorganization was attributed to the liquid crystal-like structure of BBPs, confirming their experimental observations [143]. There are also a number of studies investigating the nematic behavior of BBPs in solutions, which do not have a complete agreement on the circumstances that can lead to lyotropic behavior. Those studies are discussed in Section 3.3.1.

Changing the architectural parameters of melt BBPs, of the same chemical composition, can affect the rheological properties [125,144]. In a study by Cao *et al.*, MD simulations integrated with analytical calculations showed that the elastic behavior of BBPs could be affected and controlled by varying the degree of the polymerization of the side chains and the number of backbone monomers between the cross-links in a BBP network [131]. Based on these factors, the elastic behavior of BBPs in a network was described in two linear and nonlinear regimes for the network deformation. In the linear regime, the shear modulus changed as a function of the degree of polymerization of the side chains, while in the nonlinear deformation regime, it was dependent on the first strain invariant and backbone deformation ratio. The elastic behavior of these networks, in the elastic regime, was found to be controlled by entropic elasticity of the BBP strands between cross-links. However, in the nonlinear deformation regime, BBP elasticity was mainly due to bending modes, and later the elongation of BBP bonds. It was also observed that increasing the degree of polymerization of the side chains led to an increase in the rigidity of BBPs due to the redistribution of the side chains upon backbone bending. The increased steric interaction between the side chains which resulted from increasing their degree of

polymerization and their redistribution, is attributed to make BBPs stiffer [131]. Cao *et al.* further integrated experimental and theoretical methods with MD simulations to find the deformation dynamic of BBP networks in melt state for different time scales indicating that the dynamic response of a network could be categorized in multiscale relaxation processes [145]. Accordingly, they showed that for the time scales below and above Rouse time [146], the relaxation behavior of BBP networks changed dramatically. They specified relaxation regimes in which the decay of shear modulus was time dependent at time scales smaller than the Rouse time of the side chains. This pointed to the internal relaxation of highly correlated side chains connected through the backbone followed by a Rouse-like relaxation of linear chains' segments. The decay or shear modulus became time independent and a function of the degree of polymerization of the backbone and side chains at time scales larger than the Rouse time of the BBP network strands. This was attributed to chemical cross-links in the system resulting in permanent stress storage. This study thus showed the importance of these time scales while designing supersoft and super elastic materials [145]. In another study, Liang *et al.* implemented MD simulations and scaling analysis to describe the relation between the shear modulus (G) of BBP networks with the strands extension ratio (β) [133]. Here, β represents the ratio of the mean square end-to-end distance of the network before deformation and the contour length of a stretched strand. It was determined that the shear modulus was directly proportional to the extension ratio following a relation $(G \propto \beta)$. This scaling relation was observed for networks with comb-like strands. However, when the grafting density was increased, the shear modulus changed according to $(G \propto \beta^{-2})$ for networks of BBPs, which indicated an increase in the stiffness and extensibility of BBPs at the same time. This was believed to be a consequence of increase in the grafting density at constant length of backbone and side chains [133].

Jacobs *et al.* studied the effect of the degree of polymerization of side chains as well as grafting density on surface and interfacial properties of BBP melts using MD simulations [132]. They demonstrated that for combs or BBPs exposed to vacuum, the fraction of backbone ends and side chain ends played a significant role in determining the surface tension. It was illustrated that when the density of end beads in grafted polymers increased, the surface tension decreased. However, the interfacial tension between linear and grafted polymer did not show any dependence on the molecular structure. This can be attributed to the fact that surface tension and interfacial properties originate from the entropic and enthalpic contributions, respectively [132]. Using MD simulations, the effect of change in the molecular topology on thermodynamic properties of BBPs in melt state was studied by Chremos and Douglas [69]. They compared segmental density, isothermal compressibility, and isobaric thermal expansion of BBPs in melt state with those from linear and branched polymers including star and ring polymer melts. It was shown that these thermodynamic properties of BBPs were quantitatively analogous to those of ring and star-like polymers rather than linear ones. The reason was that these properties are primarily dependent on molecular shape parameters including size, softness, etc., and their topology could only be effective if it changed the average molecular shape [69].

Several experimental and computational studies have investigated the packing of BBP backbones in melt as well as in solutions [69,145,147–149]. They considered a mesh-like structure for BBPs, formed by the interpenetration of BBP side chains, characterizing these networks with a characteristic correlation length using experimental approaches like small angle neutron scattering (SANS) [150]. This characteristic length is specified by the correlation peak in the scattering and was shown to scale with the degree of polymerization of the side chains [69,147,148]. Similar characteristic features have also been reported for polyelectrolytes in solution [151]. In this connection, Sarapas *et al.* studied uncharged BBPs in melt state as well as highly charged BBPs in solutions using an experimental approach integrated with MD simulations [150]. The results of simulations and neutron scattering measurements showed that these chemically different BBPs showed correlation peaks in melt state and solution. The peak position for uncharged BBPs in melt state suggested that the correlation length (ξ) scaled with backbone concentration (C_{BB}) as $\xi \sim C_{BB}^{-0.47}$. Similarly, for bottlebrush polyelectrolytes scaling was $\xi \sim C_p^{-0.5}$ where C_p represented the concentration of bottlebrush polyelectrolytes. Moreover, they showed that lowering the grafting density of uncharged BBPs in melts led to wider correlation peaks, which was attributed to the packing disparities between BBPs with high and low grafting densities. Similarly, increasing salt concentration in semi dilute solutions of bottlebrush polyelectrolytes resulted in broadening of the correlation peaks [150].

3.2. Molecular conformation on surfaces

BBPs grafted on surfaces provide a broad range of distinct applications including lubrication [6], antifouling [152] and antimicrobial [153] coatings that can also tune the wettability of surfaces [10,153]. Hence, gaining a deep insight into the role of BBPs in these applications is necessary in order to tailor the properties of surfaces and BBPs as desired. In this connection, we discuss the computational studies that focus on understanding the prominent factors affecting BBP conformations on surfaces and their relevant properties.

There are a number of computational reports that have discussed the dependence of BBP conformation on the adsorption energy on surfaces [111,112,154]. The investigation of BBP adsorption on a solid surface using MC simulation by Hsu *et al.* demonstrated that the strength of adsorption energy was one of the determining factors for the conformation of the BBPs near surfaces [111]. By changing the strength of adsorption energy, they found out that for energy values slightly lower than a critical value, BBPs maintained a three-dimensional conformation. While for energies greater than the critical value, a transition to a quasi-two-dimensional conformation occurred. This critical energy was equal to the energy at which the adsorbed linear chains, on a surface, transformed from a three-dimensional to a two-dimensional conformation. Increasing the short-range attractive energy caused the side chains to get closer to the surface and adsorb easily. Adsorbed side chains with longer lengths, dragged other "unadsorbed" BBP chains toward the surface. They speculated that the complicated cooperative interplay between the chains and backbone caused the adsorbed chains to have a feedback effect on the unadsorbed parts of the backbone to drag them toward the surface [111]. A follow-up study by Hsu *et al.* further illustrated the relationship between the adsorption energy and the mean distance of backbone monomers from the substrate. They showed that the adsorption of backbone monomers increased drastically as the adsorption energy increased beyond 1.25, due to stronger interactions between BBPs and the surface (Fig. 4A) [154]. In another MC simulation study by Wernersson and Linse, it was demonstrated that at low grafting densities, the adsorption of side chains on the surface caused BBPs to spread on the substrate. This resulted in the backbone alignment parallel to the substrate.[112] On the other hand, increasing the grafting density increased the repulsion between the chains causing some side chains to desorb from the surface. A further increase in grafting density increased the repulsive intermolecular interactions, which desorbed the side chains from the surface. This further resulted in a perpendicular alignment of the BBP backbones to the surface. Consequently, at high grafting densities, any interaction strength between the side chains and the surface led to the formation of polymer brushes [112].

The results of MC simulations conducted by Flikkema *et al.* focused on understanding the effect of rigid side chain attraction on the conformation of BBPs adsorbed on a surface [155]. They observed that for BBPs with rigid backbones, when the interaction energy between side chains exceeded a critical value, the side chains collapsed onto the backbone. In this case, the side chains were allowed to rotate around a hinge point or move to a new location in an isotropic way. On the other hand, for a flexible backbone, in MC simulations, they used three types of Monte Carlo moves for the side chains, including pivot moves, shifts

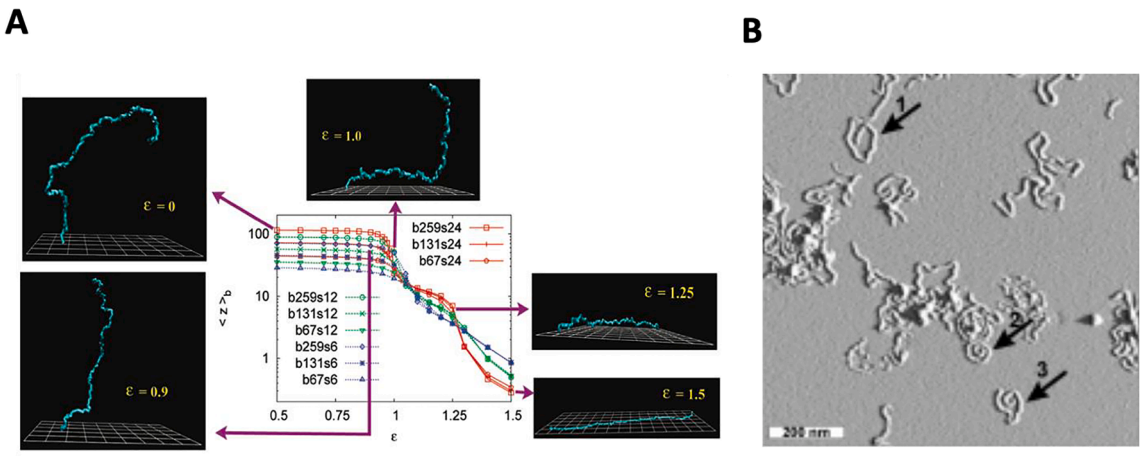

Fig. 4. A) Average position $< z >_b$ of backbone monomers plotted versus adsorption energy ε for several choices of backbone chain length N_b and side chain length N (denoted as bN_bsN in the Figure). For the case $N_b = 131$, $N = 24$ and five choices of ε, typical snapshot pictures of the backbone chain are shown, as indicated. Note that for each effective monomer, only the z coordinate of the four lower sites of the cube is counted. Note the logarithmic scale of the ordinate in the Figure. *Reprinted with permission from* [154] *Copyright (2011) American Chemical Society.* B) SFM micrograph of individual cylindrical brushes lying flat on the mica surface. The arrows show one of the typically observed conformations – 2d helices of tightly winded cylindrical brushes. *With kind permission of The European Physical Journal (EPJ) and* [157].

and flipping moves, although in some cases the flipping movement was not included. When the side chains were allowed to flip from one side of the backbone to the other side, the attraction between the chains caused the aggregations of several chains along the backbone. This resulted in the local folding of the backbone, and a decrease in BBP persistence length in both cases that the side chains were allowed to flip or not [155]. Persistence length is a characteristic length used to specify the intrinsic stiffness of a polymer [34]. Specifically, in the context of the backbone of BBPs, it has been defined as the length of the chain section that remains straight [156]. Another study by Khalatur *et al.*, demonstrated that for the BBPs strongly adsorbed on a surface, the distribution of side chains around the backbone played an important role in the final conformation of BBPs [157]. For an asymmetric distribution of side chains along the backbone, with more chains accumulated on one side of the backbone, an unusual helical structure of the BBP was observed, even for good solvent conditions. This observation was attributed to the excluded volume effect of the long side chains, which caused BBPs to wind and form a helix-like structure. The scanning force microscopy micrographs gained through an experimental procedure for poly(methyl methacrylate) on a mica substrate confirmed the formation of the helix-like BBPs (Fig. 4B) [157].

It has been shown that the properties of a surface with a polymer film are dependent on the intrinsic properties of the polymer like density, molecular mass, polymer dispersity, as well as the molecular packing at the interface [158,159]. Accordingly, understanding the structure of BBPs at surfaces in the presence or absence of solvent is of prime importance for tuning the wettability of the surfaces, one of the prominent applications of BBPs on surfaces [70]. Chang *et al.* studied the effect of BBP molecular weight on the orientation of side chains and backbone monomers, and consequently its effect on the hydrophobicity of surfaces coated with BBP films. They used AA and CG MD simulations to investigate the distribution of side chains and backbone monomers at the polymer-air interface in thin films of partially fluorinated BBPs [70]. According to the CG MD simulations, the side chains accumulated at the polymer-air interface parallel to the substrate, while the backbones remained in thin film bulk due to the entropic reasons. Specifically, they showed that alignment of the fluorinated side chains at the interface resulted in the minimizing the entropy. AA MD simulations were used to study the detailed atomic composition of fluorine atoms on the surface. Comparison of these AA MD simulations with experiments further revealed that increasing the molar mass of polymers led to an increase in the existence of fluorine atoms at interface but severely hampered the tunability of the contact angle and surface energy [70].

Elli *et al.* performed off-lattice CG MC simulations to investigate the effect of branching density of highly grafted polymers on the adsorption of BBPs on a surface [116]. They showed that the number of end-beads increased due to increase in branching but many of these additional beads did not adsorb on the surface due to the entropic reasons. This further resulted in decrease in the interaction energy between BBPs and surface compared to between linear polymers and surface. However, they showed that even at a weak adsorption strength, the persistence length of backbone increased significantly. It was also shown that an increase in the grafting density enhanced BBP aspect ratio and persistence length, which was considered as a potential reason for experimentally observed liquid-crystalline behavior of BBPs on flat surfaces [116,160]. In addition, off-lattice MC simulations carried out by Saariaho *et al.* highlighted the effect of side chain length on the equilibrium conformations and persistence length of BBPs in a film confined between two parallel surfaces [113]. When the distance between the surfaces was reduced from infinity to zero, the BBP conformation changed from a 3D to 2D structure. It was observed that for the molecular brushes in a 2D system, the ratio of persistence length to BBP diameter increased for longer side chains. However, this ratio, a determining factor for exhibiting lyotropic behavior [161,162], was almost constant for a 3D system. They attributed this behavior to the weaker intramolecular excluded volume effect in a 3D conformation rather than a 2D situation, and believed that stronger excluded volume interaction between the monomers could lead to increased persistence length. Hence, they suggested that for a 3D system of BBPs, the ratio of persistence length to BBP diameter may only be affected by much longer side chain lengths than what they studied [113,163].

Using MD simulations, Carillo *et al.* investigated the effect of grafting density, compression and shear stresses on the lubrication properties of neutral and charged BBPs [164]. It was observed that upon subjecting charged BBPs grafted on a surface to shear stress and compression by another surface, the backbone deformation dominated the deformation of the BBPs due to the electrostatic interaction between charged monomers. On the other hand, neutral BBPs exhibited the deformation of both backbone and side chains. The backbone deformation ratio was shown to be dependent on the grafting density and compressive stress, causing the shear viscosity to vary with applied shear rates. It was also indicated that for both charged and neutral BBPs, increasing shear rates resulted in a rise in friction coefficient [164,165].

Panyukov *et al.* employed MD simulations and showed that the

strong adsorption of BBPs, spreading on a substrate, caused significant backbone tension amplification [3]. This tension was dependent on the grafting density, side chain length and spreading parameter - the tendency of the BBP to cover area on the substrate and "wet" it. These aforementioned parameters could affect the BBP conformation on the substrate as well as the extension of the side chains. To illustrate the point, in this study, increasing the grafting density made the side chains more stretched, and the relevant tension of side chains was transmitted to backbone monomers leading to the tension amplification of the backbone [3]. They also showed that depending on the spacer length between side chains and the spreading parameter, BBPs adopted various conformational regimes [3]. However, the dependence of backbone tension on these parameters varied for each of the conformational regimes [3]. For BBPs tethered on a substrate, Leuty *et al.* used bead-spring CG MD simulations to study the effect of molecular crowding on the tension accumulated on the BBP backbone [166]. It was found that for low BBP coverage on the surface, as the side chains merely interacted with other chains from the same backbone, the intramolecular interaction was the only determining factor on tension accumulation of the backbone. Moreover, increasing molecular crowding contributed to increasing intermolecular as well as intramolecular interactions. This led to a considerable rise in backbone tension, resulting in a perpendicular orientation of the extended side chains to the surface [166]. Paturej *et al.* performed MD simulations using a bead-spring model, and showed that a strong adsorption of BBPs on surface led to the breakage of the bonds between monomer beads [163]. They demonstrated that the mean lifetime of the covalent bonds between backbone monomers was reduced significantly upon strong adsorption due to the increased amount of tension on the backbone [163]. Moreover, increasing the grafting density and side chain lengths also drastically reduced the mean lifetime of covalent bonds owing to the steric repulsion between the grafted polymer side chains [163].

3.2.1. Segregation of BBPs on surfaces and interfaces

Blends of polymers in thin films can cause surface segregation, causing the composition of polymer blends near the interfaces of a thin film to be different from that of the bulk [121]. Coatings consisting of BBPs, in the presence of linear chains, can also segregate near the interface. As this property of thin film blends is vital for practical applications like tuning the wettability of the surface [121], many studies have focused on understanding this behavior and investigating the determining factors causing surface segregation [167–171]. Teng *et al.* used DPD simulations to study the effect of BBP architecture on surface segregation in a thin film including BBPs and linear polymers, when the film was confined between two parallel walls [106]. It was observed that BBPs aligned with the walls, and more importantly, BBPs with larger persistence lengths were more likely to accumulate near the walls because they could be aligned with the walls to stay in the depletion zone generated near the interfaces. Consequently, this resulted in a reduction of the system free energy prevailed by translational entropy. The degree of surface segregation was further investigated by analyzing the volume fraction occupied by BBPs along the film thickness. An increase in the grafting density also resulted in a higher concentration of BBPs near the surfaces [106]. A study by Mei *et al.* revealed that the blend of polystyrene (PS) and poly(methyl methacrylate) (PMMA) bottlebrush copolymers and the same linear homopolymers in a thin film on a substrate caused surface segregation of BBPs [121]. Experimental investigation integrated with SCFT simulations showed that BBPs were more likely to be found at the film-air interface due to the entropic and enthalpic preference of BBPs near the interfaces and the repulsive forces between copolymers. It was also demonstrated that when the molecular weight of the linear polymer was above a critical value, surface segregation was observed in the film [121]. Mah *et al.* further demonstrated that the degree of polymerization of side chains and backbone of BBP as well as the degree of polymerization of the linear polymers altered the segregation behavior in thin films of polymer blends [172]. They systematically varied these parameters to investigate the effect of changing these architectural parameters on phase behavior of polymers. The results led to phase diagrams illustrating the segregation of BBPs as a function of N_b/N_{sc} -and N_m/N_{sc} .where N_b, N_{sc}, and N_m represented the degree of polymerization of the backbones, side chains and the linear polymers, respectively. BBP depletion or enrichment on the film-air interface or even an equal distribution of BBPs and linear polymers at the interface were three types of segregation at the film interface [172].

3.3. Molecular conformation in solutions

Various computational studies have been presented in literature to accurately predict conformational properties of BBPs in solution [12,89,173]. Dutta *et al.* developed the wormlike cylinder (WLCy) model to describe BBPs with flexible backbone and side chains in a dilute solution [89]. They used a hybrid BD/MC based fine-grained model with explicit side chains to represent a molecular-level BBP structure. Four quantities obtained from this fine-grained model, namely, end-to-end distance $\langle R^2 \rangle$, radius of gyration $\langle S^2 \rangle$, hydrodynamic radius R_H, and intrinsic viscosity [η], were consistently reproduced by a systematically parameterized WLCy model. Moreover, they also showed that the WLCy model is consistent among a wide range of conformational and dynamic properties and for a large number of polymer architectures (e.g., side chain length, backbone length, and grafting density). Overall, WLCy could reproduce the behavior of the more detailed CG model through appropriate mapping of parameters and thus, can be useful for large-scale simulations of bottlebrush suspensions. The schematic procedure of developing this model is illustrated in Fig. 5A [89]. In a follow-up study, they developed a CG model for BBPs with implicit side chains to study force-extension behaviors of bottlebrush architectures. They employed CG MC simulations to provide an insight into the BBP elastic behavior when they were subjected to stretching under various circumstances, like the flow-induced stretching in solutions [174]. The simulation results were compared with the aforementioned model of BBPs with explicit side chains and showed two stretching regimes for BBPs. They demonstrated that for low pulling forces, linear and non-linear force-extension regimes were observed for the stretched cylindrical BBPs in response to the applied force, and the extension behavior of BBP could be captured using the developed CG model. However, at high pulling forces, the application of CG model was shown to be insufficient because the backbone was stretched in the length scales less than that of a CG bead, while, at low forces, the overall structure of BBP was stretched. Hence, using the model with explicit side chains seemed necessary to capture BBP behavior at high forces [174].

The elastic behavior of BBPs in a solution can be tuned by altering structural parameters or the environmental factors like concentration or the quality of solvent [174–176]. Zhulina *et al.* presented a scaling theory investigating BBP structure and their elasticity behavior within a wide range of concentrations [175]. They showed that even for two BBPs with the same number of chains and equal lengths of backbone and side chains, the elasticity differed owing to the intramolecular structural rearrangement in dilute and in semidilute solution regimes [175]. Jacobs *et al.* investigated the effect of branching on the elasticity and swelling of BBP networks, and compared them to linear chain networks [176]. Using a combination of MD simulations, theoretical and experimental methods, they observed that BBP networks exhibited much stronger swelling than linear polymers due to architectural disentanglement of BBPs in networks and stronger interaction between the bulkier BBPs and solvent molecules. Moreover, they illustrated that the shear modulus, which was dependent on BBP deformation, changed as a function of the swelling ratio. They attributed this behavior to the dependency of the swelling on both the three-body repulsion and the elasticity of the network. Considering the relationship of BBP architecture with swelling modulus and elastic modulus, controlling BBP architectural parameters could lead to the design of superabsorbent materials [176].

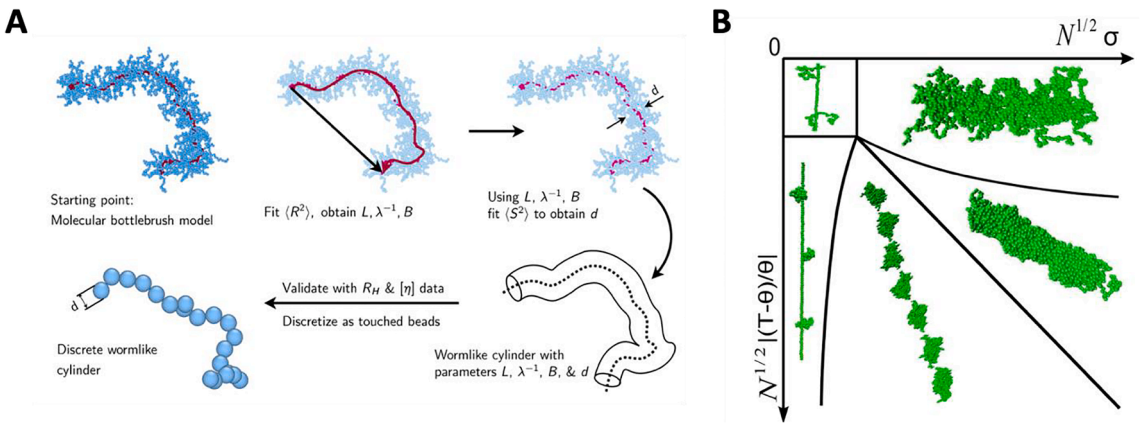

Fig. 5. A) Schematic showing the extraction of model parameters from the bottlebrush simulation data. Fine-grained models using explicit side chains are first systematically parameterized by fitting $\langle R^2 \rangle$ using the length L, Kuhn length λ^{-1}, and excluded volume parameter B. Subsequently, the diameter d is determined from fitting the R_g $\langle S^2 \rangle$. This sets all the parameters for the wormlike cylinder model, which can then be validated with predictions for hydrodynamic radius $R_H$and intrinsic viscosity (η). Once we have a consistent set of wormlike cylinder parameters, we can use these to represent a bottlebrush with an implicit side chain model based on a discrete wormlike cylinder. *Reprinted with permission from* [89]. *Copyright (2019) American Chemical Society.* B) (Colour on-line) Schematic phase diagram of a bottlebrush polymer with a rigid backbone under poor-solvent conditions, in the plane of variables $\times = N^{1/2}\sigma$ and $y = N^{1/2}T - \theta|/\theta$, where θ is the θ-temperature separating the good-solvent regime (T > θ, not shown here) from the poor- solvent regime. The lines separating the different regions have been proposed by Sheiko *et al.* [193] but are not to be understood as quantitative estimates of phase transition lines, but rather as rough estimates of smooth crossovers. Representative snapshots from the simulations obtained in the present work give evidence for the existence of the proposed states, where the side chains form either isolated objects (left two regions), which may be either collapsed globules (lower leftmost region) or still almost Gaussian coils (upper leftmost region), and for cylindrical brushes, either stretched (upper right region) or collapsed (lower rightmost region). The lower central region shows a pearl-necklace structure, which has a nontrivial almost periodic mesophase order along the backbone. *Reprinted with kind permission of Europhysics Letters (EPL) and* [21].

3.3.1. The relationship between BBP concentration in solutions, persistent length and lyotropic behavior

The persistence length is a characteristic length specifying the stiffness of the polymer, and in the context of BBPs can be defined as the distance over which the vector tangent to the backbone chain is correlated [177,178]. Because the persistence length of the backbone and the overall molecular brush in solutions plays a significant role in determining the conformation of BBPs, several theoretical and simulation studies have investigated the factors affecting the persistence length [23,37,122,179]. Many studies reported that increasing side chain lengths contributed to a drastic increase in the persistence length of backbone and the overall BBP [37,180–185]. In theoretical studies, this was attributed to the increased repulsive interactions between the side chain monomers, known as the excluded volume effect [180,186,187]. In this regard, MC simulations by Saariaho *et al.* [156] of BBPs in a dilute athermal solution (low concentration) were performed, where the polymer and solvent molecules are assumed to have no energetic interactions [188,189]. This study indicated that side chain topology played a significant role in the enhancement of the persistence length of the polymer [156]. Specifically, they changed the side chain topology by varying the diameter of beads in the side chains and showed that it enhanced the BBP persistence length due to excluded volume interaction between side chains. Moreover, increasing the size of the beads resulted in an increase in the ratio of persistence length to BBP diameter. As this ratio is known to play an important role in determining the lyotropic behavior, their study suggested that choosing the right chemistry of side chains may contribute to a desired lyotropic behavior of BBPs. Interestingly, these authors showed that the ratio of persistence length to BBP diameter was approximately independent of the side chain length and did not change as a function of the side chain length [156]. The results of MC investigation integrated with experiments by Rathgeber *et al.* revealed that increasing the backbone length as well as the length of side chains (up to half of the backbone length) resulted in a more stretched structure, leading to an increased persistence length of backbone [115]. They showed that although the ratio of persistence length to the diameter of BBP was low (~4) in their experiments, a lyotropic behavior was observed at low polymer concentrations [115]. This observation was in contrast with the previously reported ratio of persistence length to BBP diameter which should be of order 10 or larger [116,190]. Rathgeber *et al.* believed that the lyotropic behavior vanished at high concentrations and attributed this behavior to the screening of the excluded volume interaction, which caused more BBP interpenetrations [115]. On the contrary, using a theoretical approach, Fredrickson predicted a lyotropic behavior at high concentrations of polymer/surfactant complex. In this study, they showed that the ratio of persistence length to BBP diameter could possibly be large enough to cause a lyotropic phase transition. They attributed this to the surfactant-induced high rigidity of the polymer/surfactant complex at high concentrations, which increased the ratio of persistence length to diameter [186]. Given the inconsistency of the results on the observation of lyotropic behavior at both low and high BBP concentrations and ratios of persistence length to BBP diameter, we believe that in addition to this ratio, other factors like the chemistry of the BBP constituents may induce the required rigidity for the formation of nematic lyotropic phase.

Hsu *et al.* employed extended MC simulations, using their previously established simulation algorithm [34], to investigate BBP characteristic length scales including R_g of side chains, backbone persistence length, and radial monomer distribution in an implicit good solvent condition [173]. Their simple cubic lattice system, based on a bond fluctuation model, efficiently reproduced the experimental values of these properties for various backbone and side chain lengths. The simulation results demonstrated that the predicted persistence length was dependent on both backbone and side chain lengths. Specifically, increasing side chain and backbone length caused the enhancement of the stiffness [173]. Using MC simulations and adopting the bond fluctuation model, Hsu *et al.*, also demonstrated that under good solvent condition, larger cross sectional diameter of BBP contributed to increase in the persistence length [114]. This observation is consistent with the aforementioned study illustrating the increase of backbone stiffness by increasing the side chain length [173].

3.3.2. Effect of architectural parameters on the conformation of bottlebrush polymers in solutions

Investigating the effect of architectural parameters on BBP

conformation in a solvent is one of the prominent purposes of several computational studies [13,35,191]. In this regard, Zhang *et al.* conducted atomistic and CG MD simulations integrated with small angle neutron scattering for BBPs with poly(norbornene) (PNB) backbone and poly(lactide) (PLA) side chains to study the effect of side chain length on the overall structure of BBP and backbone dynamics [35]. They revealed that increasing the side chain length from 5 to 10 monomers caused the BBP structure to change from a flexible chain-like structure to a compact form, contributing to a reduction in the R_g. They attributed this behavior to the solubility difference of side chains and backbone in tetrahydrofuran. Since tetrahydrofuran was proved to be a better solvent for the side chains compared to the backbone, increasing the length of side chains could allow them to encapsulate backbone monomers. This resulted in the formation of an overall condensed shape. However, a further increase in side chain lengths (>10 monomers) resulted in a rise in the R_g because all the free spaces around BBP was already occupied by the compacted side chains [35].

Theodorakis and Fytas utilized MD simulations to elucidate the effect of structural parameters on the conformation of flexible backbone and side chains under theta solvent and good solvent conditions [12]. The solvent quality was altered by changing the temperature in the range of $T = 3$ *to* $4\ \varepsilon/k_B$, where T≈3.0 and 4.0 represent theta and good solvent conditions, respectively. They showed that increasing the grafting density, side chain length, and temperature caused the backbone monomers to have a more cylindrical symmetry. The reason for this behavior was attributed to longer side chains and higher grafting densities that contributed to a more stretched and stiffer backbone to the point that the end beads of backbone could barely get close to each other. Additionally, increasing the temperature to approach 4.0, which represents a good solvent condition, enhanced the affinity of the monomers with the solvent to make it more stretched. They illustrated that even at temperatures close to the theta point, BBPs could form stretched conformations, suggesting a weak dependence of linear dimensions of BBPs on the quality of solvent [12]. In another study, they elucidated the effect of solution temperature and solvent quality on the conformations of BBPs in poor solvent condition [191]. They showed that at low temperatures, which corresponded to the poor solvent condition, the side chains collapsed and BBPs adopted a spherical structure. In this case, the total number of monomers was the only effective parameter on the molecular structure. However, at higher temperatures, depending on grafting density as well as the number of monomers in backbone and grafted side chains, BBPs experienced a transition of conformation from spherical to coil-like or cylindrical structures. Smaller backbone and side chain lengths, coupled with low grafting density resulted in a coil-like structure, while increasing these parameters enabled the monomers to arrange more homogeneously around the backbone. In addition, increasing the length of the side chains caused steric repulsions between monomers, causing the side chains to become more stretched [191].

Theodorakis *et al.* used MD simulations to investigate the structural transition of BBPs with flexible side chains and rigid backbones in an implicit poor solvent condition [192]. They found that at low grafting densities, side chains collapsed, and formed pearl-like shapes where each pearl included just one grafted side chain. Increasing the grafting density led to the formation of the pearls containing several side chains clustered together. The formation of these pearl-necklace structures can be attributed to increased interaction between the side chains as the grafting density increased. As temperature increased, this transition to the pearl-necklace structures occurred for even lower grafting densities, which may be attributed to larger fluctuations at a higher temperature. Similar behavior was also predicted by a scaling law in another study by Sheiko *et al.* [193]. For intermediate grafting densities, these pearls contained several side chains and appeared like non-spherical ellipsoidal shapes. At high grafting densities, an overall cylindrical structure of BBP with side chains homogeneously positioned along the axis was reported [192]. The gradual crossover between these structures was represented in a phase diagram as a function of side chain length, grafting density and temperature, and the interplay between these parameters determined the BBP conformation in solution (Fig. 5B) [21]. Another similar study by Theodorakis *et al.* on bottlebrush copolymers with rigid backbones in a poor solvent illustrated a microphase separation between the side chains. This resulted in a conformational transition of a BBP from pearl-necklace structures at low grafting density to Janus dumbbell structures at high grafting density. This behavior was attributed to the microphase separation and clustering of the side chains at the same time [194]. This study also showed that the phase transition occurred gradually in solutions, whereas it was sharp in bulks or copolymeric melt BBPs [194]. Polotsky *et al.* integrated MC simulations with a field-theory-based approach to study BBPs with a solvophobic block of chains inside (core) and a solvophilic block in the outer layer (shell) of the molecular brush [195]. They showed that changing the solvent quality from theta to poor solvent for the inner chains could contribute to the collapse of the core. When the strength of the solvent for the core chains was decreased, the pearl-necklace structure was observed in the inner part of the BBP. They also suggested that this behavior was due to the insolubility of the core in the selective solvent. The experiments conducted on core–shell BBPs with poly(acrylic acid) as the core and poly(n-butyl acrylate) as the shell confirmed the validity of this structural transition in simulation results [195].

The amphiphilic copolymers have attracted much attention due to their unique properties in solution, in bulk, and at interfaces [196]. Several computational studies have investigated their microphase separation under poor solvent conditions [194,197,198]. MC simulations conducted by Jong and Brinke showed the formation of Janus cylinders resulted from phase separation of BBPs with two incompatible chain types [199]. They observed that under poor solvent condition, when BBPs were restricted to have rigid backbones, the side chains of the Janus cylinder structure transitioned into a pearl necklace structure. Although, for BBPs with flexible backbones, side chains of the same type collapsed and formed multiple globules [199]. Erukhiomovich *et al.* used analytical theory and MD simulations to study BBPs with stiff backbone and flexible chains in a poor solvent to show that changing the ratio of interaction energy between dissimilar and similar monomers played an important role in their microphase separation, and changing this ratio could lead to the formation of Janus-cylinder structures [5].

4. Stimuli-sensitive polymer simulations

Stimuli-sensitive polymers are defined as polymers that produce observable micro- or nanoscale changes in their morphologies or molecular structures in response to environmental triggers such as temperature, pH, electric or magnetic fields, mechanical force and even light [63,200–203]. Due to these special properties, these “smart-polymers” have found several applications as sensors and biosensors [204], controlled drug delivery [205], environmental remediation [206], etc. BBPs grafted with such polymer side chains present an interesting group of macromolecules in the form of stimuli-sensitive BBPs, which usually display varied phase behavior, solution conformations and interfacial properties in response to a change in surrounding environment [207,208]. Although little experimental and computational research has been carried out on these BBPs, these macromolecules provide an ease of structural tunability unmatched by conventional BBPs, which can be utilized in generating application-oriented system properties [209]. This makes them hot candidates for future experimental and computational research. In this section, we review two computational studies available in literature on different stimuli-sensitive BBPs.

One of the best known examples of stimuli-sensitive polymers is a thermosensitive polymer named poly (*N*-isopropylacrylamide) (PNIPAM) [202,210,211]. Bejagam *et al.* studied PNIPAM-based BBPs in water using CG MD to determine the effect of grafting density, backbone and side chain lengths, and temperature on the conformational evolution of the BBPs and its side chains [16]. These MD simulations were performed using explicit solvent models at 290 K and 320 K, which are

below and above the lower critical solution temperature (LCST) of PNIPAM, respectively. The results indicated that for relatively short side chains (5 and 10 monomers), the PNIPAM side chains appeared like elastic rods, and did not show much difference at the two temperatures. However, for longer side chain lengths (18 and 30 monomers), and grafting density up to 50%, these side chains underwent a coil-to-globule transition above the LCST, due to which the BBPs resembled somewhat cylindrical and spherical shapes for the temperatures below and above LCST, respectively. When the grafting density was increased to 100%, PNIPAM side chains displayed a globule-like conformation at both 290 K and 320 K as a result of the dehydration of side chains due to steric effects. (Fig. 6A (i-ii)) Conformational changes in the grafted PNIPAM side chains also affected the overall BBP conformation with a bending of the hydrophobic backbone observed at lower grafting densities [16].

A recent study by Chang *et al.* employed DPD simulations to study the self-assembly behavior of comb-like graft copolymers with pH-sensitive hydrophilic side chains [105]. The self-assembled systems exhibited a variety of morphological conformations including worm-like and sheet-like micelles, as well as porous, unilamellar and multilamellar vesicles. The influence of pH was realized through solvent quality (α-$_{AS}$) where neutral pH depicted poor solvent (larger α-$_{AS}$) and higher or lower pH indicated good solvent (smaller α-$_{AS}$). It was observed that micellar aggregates were formed at smaller α-$_{AS}$ values, which converted to unilamellar vesicles (ULV) at low concentrations with an increase in α-$_{AS}$ values. The size of vesicles increased with increasing concentration. As pH approached a neutral value (large α-$_{AS}$ value), ULVs converted into multilamellar vesicles (MLV) with a layer by layer structural addition, similar to that of an onion as shown in Fig. 6B (i-ii). The water permeation through the formed structures was also studied with the membrane permeability observed to reduce as ULVs converted to MLVs. The controlled release of two types of drugs with distinct hydrophobicities situated at different layers of the MLV was also examined [105].

5. Molecular conformations of bottlebrush polyelectrolytes

BBPs can be classified as neutral or polyelectrolyte polymers based on the charge on their grafted side chains [212]. The long-range interactions between charged monomers play a crucial role in determining the conformation of polyelectrolytes. As a consequence, many studies

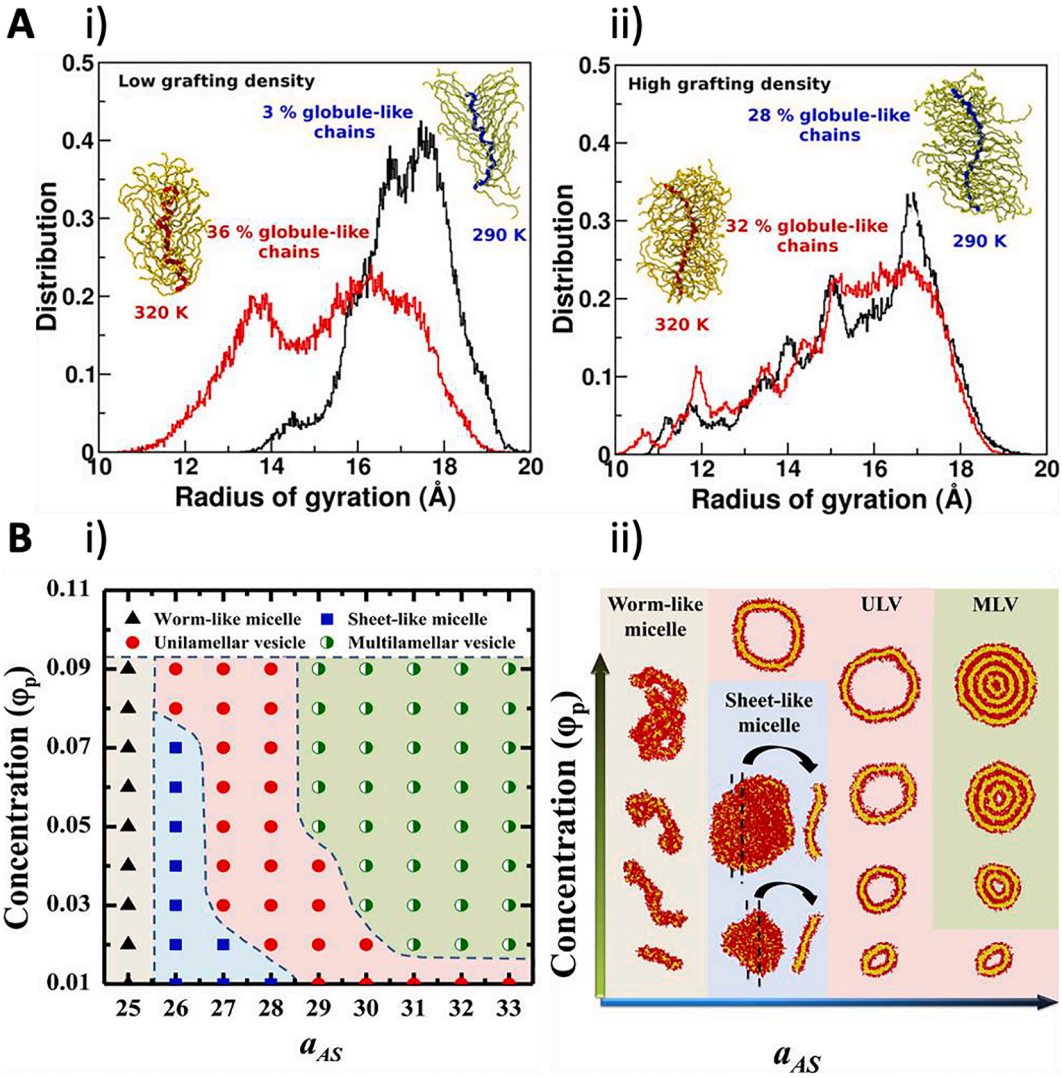

Fig. 6. A) Snapshots and normalized distribution of R_g, averaged over all the side chains for thermosensitive BBPs with (i) Low grafting density and (ii) High grafting density. The backbones of BBPs were represented in blue and red at 290 and 320 K, respectively. *Reprinted with permission from* [16]. *Copyright (2019) American Chemical Society.* B) (i) Morphological phase diagram of aggregates formed by comb-like copolymers as a function of polymer concentration (φ_p) and pH value (a_{AS}). (ii) Characteristic morphological snapshots illustrated for various polymer concentrations (φ_p) and pH values (a_{AS}). *Reprinted with permission from* [105]. *Copyright (2013) American Chemical Society.* (For interpretation of the references to color in this figure legend, the reader is referred to the web version of this article.)

have shown that in comparison with neutral brushes, polyelectrolyte brushes exhibit different behaviors [213–218]. The degree of ionization of the monomers, the valence of counterions, and the structural features are important to control the conformation of polyelectrolyte BBPs and their relevant properties [22,219,220].

Cao *et al.* employed MD simulations to investigate the effect of electrostatic strength on the conformational transitions of a single polyelectrolyte BBP consisting of both neutral and charged side chains [212]. They revealed that the Bjerrum length [221] - the distance at which the electrostatic interaction energy competes with thermal energy - has a considerable effect on the conformation of the side chains. Neutral side chains in a poor solvent formed clusters with various sizes as a consequence of increasing the Bjerrum length. These clusters could aggregate to form one single cluster as a result of further increase of electrostatic interaction. Consequently, at large or very small Bjerrum lengths, the polyelectrolyte BBPs resembled a globule-like structure with a core of neutral side chains. The formation of this structure was attributed to the strong attraction between neutral side chains in a poor solvent and the weakening of electrostatic interactions due to the counterion condensation at a large Bjerrum length. However, in a good solvent, clusters of neutral side chains did not appear. And the globular structure of polyelectrolyte BBPs with a core consisting of charged side chains could only be formed at large Bjerrum lengths. These structural transitions were attributed to the competition between electrostatic energy and the short-range Lennard-Jones potential [212].

Carrillo and Dobrynin investigated the effect of grafting density and side chain length as well as the electrostatic interaction on the thickness of polyelectrolyte BBPs tethered to a surface [22]. It was elucidated that longer, flexible side chains contributed to form brush layers with larger thickness, while increasing grafting density led to a decrease in thickness. This reduction in the thickness continued until it reached a saturation and retained that thickness over a wide range of grafting densities. They attributed this behavior to the contraction of the side chains as a consequence of increase in the grafting density, which caused decrease in the repulsion between side chains due to the counterion condensation [22]. However, it was previously shown that for polyelectrolyte BBPs with rigid side chains, increase in the grafting density led to an increase in thickness [222]. Borisov and Zhulina employed mean-field theory to predict the conformation of polyelectrolyte BBPs in salt-free solutions [220]. They demonstrated that increasing grafting density or/and increasing the number of charged monomers led to stretched polyelectrolyte BBPs due to the accumulation of the counterions in intramolecular spaces [220].

Linse and Claesson used mean-field theory to investigate the effect of side chain length on the adsorption of bottlebrush polyelectrolytes on mica and silica substrates with negatively charged surfaces [223]. The BBP backbone consisted of charged segments, where the percentage of these charged segments (X) ranged from 0 to 100. The mica surface had no electrostatic interaction with BBP, while the silica-like surface was considered to have positive affinity to the BBP chains. Surface excess, which was defined as the amount of adsorbed polymer on the surface, was shown to be dependent on X. The results revealed that for the mica-like surface, increasing the length of side chains led to a decrease in the surface excess at small X. This behavior demonstrated the dominance of the entropic repulsion between the chains and also between the surface and the side chains. On the contrary, for a large X, increasing side chain length contributed to increased surface excess. However, for the silica surface, the surface excess increased for any value of X as a result of increasing side chain length. This behavior was attributed to the favorable interactions between the chains and the surface [223].

Although various simplifications can be applied to polyelectrolyte BBPs, they are sometimes too complex to be described by analytical theories [30]. Therefore, a model based on SCFT can be applied to investigate the conformation of BBPs on the surface [30]. Feuz *et al.* used SCFT to investigate the interactions between polyelectrolyte BBPs, which had hydrophilic and neutral side chains tethered to a backbone of polyelectrolyte monomers [30]. It was shown that the adsorption of these macromolecules on the oppositely charged surface mostly depended on the molecular architecture parameters such as grafting density and the length of side chains. Changing the grafting density and the degree of the polymerization of the side chains affected the electrostatic interactions between the backbones of the BBPs and the surface. At high grafting density and short side chains, the polyelectrolyte BBP could be adsorbed strongly on the substrate, while low grafting density and long polymeric side chains resulted in the steric repulsion of the side chains from the surface. At intermediate grafting densities, the relation between screening length [224] - a characteristic length of electrostatic interactions between charged particles to the thickness of the molecular brush - controlled the adsorption or depletion of the BBP to the surface [225].

Rusaano *et al.* performed MD simulation to study the different behaviors of charged and neutral brushes tethered to two parallel surfaces [219]. They indicated that the disjoining pressure, which is the interactive force between substrates per unit area, is related to the required bending energy of polyelectrolyte BBPs compressed between grafted substrates. The pressure increased with a reduction in the distance between these surfaces. However, this dependency was weaker in the case of polyelectrolyte BBPs compared to neutral brushes. This behavior of polyelectrolyte BBPs was attributed to the interaction between counterion clouds, which hampers a strong overlap between brush polyelectrolytes [219].

6. Self-assembly of BBPs

The tunability of the structural parameters of BBPs has created a context for their self-assembly into various morphologies due to microphase separation in solution, melt, and on surfaces [4,226,227]. Several studies have demonstrated that BBPs with block copolymers can undergo a quick phase separation, and form microdomain self-assembled structures [122,228,229]. Investigations on the self-assembled structures revealed that both structural parameters of BBPs and solvent quality control this process. The self-assembled structures of BBPs exhibit distinct properties, which may not be easily achieved using linear polymers. For example, unlike linear polymers, BBPs can self-assemble to create nanostructures up to several hundred nanometers, with large domain periods, making them suitable to be applied as photonic crystals [227,230–232]. In addition, the critical micelle concentration for BBPs can be significantly lower than that of analogous linear polymers owing to the larger size of BBPs [226]. Moreover, recent advances in synthesis of branched polymers including BBPs have set the stage for attracting tremendous attention toward the self-assembly of BBPs. In this regard, a wide variety of the potential applications provided by the assembly of these brush polymers are reviewed in articles [41,233].

6.1. Factors affecting the self-assembly of BBPs

Many computational studies have investigated the effect of various factors including structural parameters, solvent quality, composition, molecular stiffness, etc. on the self-assembled structures of BBPs to specify the factors determining the formation of desired micro- and nanostructures. Gumus *et al.* utilized DPD simulations to investigate the self-assembly of amphiphilic BBPs with incompatible side chains when the solvent quality was suddenly changed [103]. They observed various non-equilibrium self-assembled structures which were formed by changing the solvent quality, the side chain length and the degree of incompatibility between the chains. The folding of side chains and the resultant self-assembly was found to be strongly dependent on the flexibility of the chains and the properties of the solvophobic core. Moreover, they demonstrated that the molecular weight of BBPs was another determining factor, which considerably affected self-assembled structures (Fig. 7A) [103]. Ahn *et al.* investigated the microphase

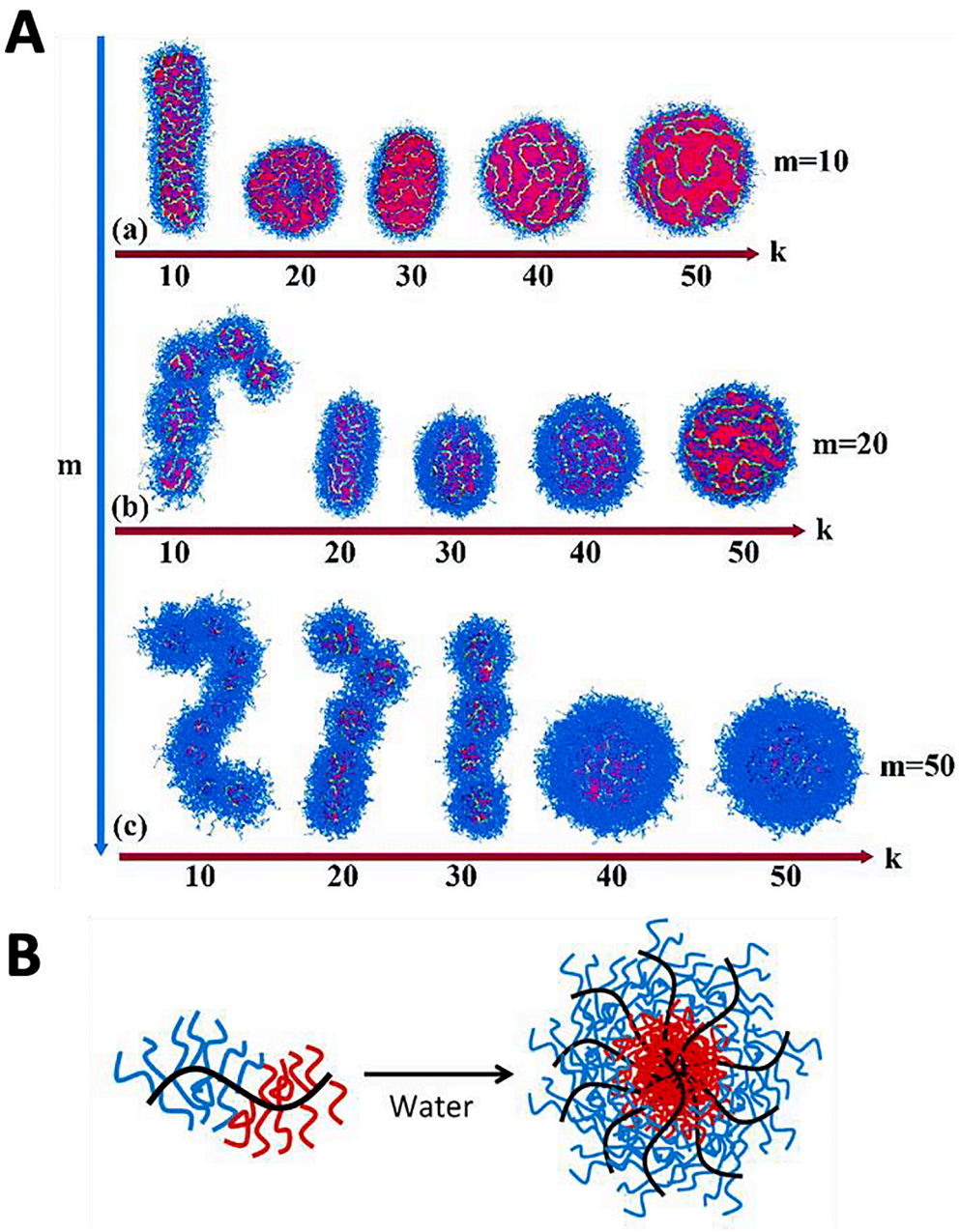

Fig. 7. A) Representative single-polymer self-assembled nanostructures obtained after a fast quench into a bad solvent condition for one of the side chains (red domains), formed by $(C\text{-}g\text{-}A_k/B_m)_{1000}$ asymmetric bottlebrushes. Solvophilic side chains are displayed in blue, whereas the bottlebrush backbone is represented by the green tube wrapping around the solvophobic cores. Solvent molecules are not displayed for clarity. The solvophilic block molecular weight is fixed at (a) m = 10, (b) m = 20, and (c) m = 50. Solvophobic side chain molecular weight, k, increases from left to right. The chemical incompatibility between A and B polymer segments was fixed at a_{AB} = 50. *Republished with permission of Royal society of chemistry, from* [103] *copyright (2020); permission conveyed through Copyright Clearance Center, Inc.* B) Schematic for the self-assembly of amphiphilic PS-PACMO bottlebrush block copolymers in water, where the red chains represent the hydrophobic PS chains and the blue chains represent the hydrophilic PACMO chains. *Reprinted with permission from* [226] *Copyright (2019) American Chemical Society.* (For interpretation of the references to color in this figure legend, the reader is referred to the web version of this article.)

segregation of BBPs consisting of poly(3-hexylthiophene) (P3HT) and poly(lactide) (PLA) side chains grafted on a polynorbornene backbone [234]. According to their results, composition of PLA and P3HT affected the morphology of self-assembled structures. BBPs with compositionally symmetric PLA and P3HT side chains, formed lamellar nanostructures with large domains. However, BBPs with compositionally asymmetric side chains showed poorly ordered morphologies or short-range ordered structures. The domain of these nanoscale morphologies of BBPs was determined by the length of PLA and P3HT side chains [234].

To investigate the effect of BBP structure on self-assembly in solution, Alaboalirat *et al.* studied the conformation of amphiphilic BBPs in solution and their self-assembly by combining small-angle neutron scattering and CG MD simulations [226]. They examined BBPs which consisted of copolymeric side chains of polystyrene and poly(N-acryloylmorpholine) (PACMO) to show that in the presence of water, the BBPs had a structure similar to a combination of globule and cylinder. However, when the number of PACMO side chains increased, BBPs formed more stretched architectures in solution. The self-assembly of these molecules formed micelles in water with a core of hydrophobic polystyrene and a shell of hydrophilic PACMO (Fig. 7B). Their analysis indicated that increasing PACMO content resulted in more stable and spherical micelles, which had a much lower critical micelle concentration compared to linear block copolymers [226]. On the contrary, Lyubimov *et al.* previously reported lower critical micelle concentration for linear amphiphilic copolymers rather than the BBPs at low solvophobicity [235]. However, the micelles formed through the self-assembly of BBPs were observed to be smaller than those obtained through the self-assembly of linear polymers [235]. Using MD simulations, Wessels *et al.* indicated that changing the molecular structure from linear or star-like polymers to BBPs led to a reduction of the size of assembled micelles and the aggregation number. Besides, the required solvophobicity for the formation of micelles was increased as a result of an increase in the number of side chains from linear polymers to BBPs [236]. Chen *et al.* employed SCFT using a worm-like chain model to probe the effect of chain conformation on the self-assembly of fully extensible block BBPs with high grafting densities, consisting of

semiflexible chains and backbone [43]. They showed that the stiffness of side chains controlled monomer packing and the conformation of the chains, and consequently played a significant role in controlling the conformation of the backbone, as well as determining the domain spacing and the sizes of the self-assembled lamellar phase [43].

It has been shown that backbone flexibility is a determining factor in the morphology of self-assembled structures [122,131]. Using CG MD simulations, Chremos and Theodorakis studied the effect of intrinsic stiffness of the backbone on the morphology of the self-assembled BBPs with block copolymers [71]. They realized that when the backbone stiffness was increased, BBPs with the same volume fraction of block A and B, and with the asymmetric side chains along backbone, transitioned from hexagonally packed cylinders to lamellar or bicontinuous morphologies. Based on the results of several simulations, morphology diagrams were provided illustrating self-assembled structures for various values of backbone stiffness (K), the length of polymer blocks (N_A, and N_B), and different numbers of the total A or B segments (M). It was shown that for the BBPs with backbone stiffness equal to zero, hexagonally packed cylinders were formed when the side chains had a remarkable difference in terms of their lengths. However, when this difference was not considerable, a lamellar structure dominated (Fig. 8). According to morphology diagrams (Fig. 8c), for $N\text{-}_A = 1$ and $N_B = M$, and for the values of stiffness equal to zero, increasing the stiffness to a value between 0.5 and 2, caused a transition from hexagonally packed cylinders to a bicontinuous structure. Besides, BBPs with a stiffer backbone (K>2) possessed a lamellar morphology. Though, when $N\text{-}_A$ was larger than M/4, increasing the backbone stiffness did not contribute to a change in the final structure [71,237]. In addition, based on BD results gained by Cao *et al.*, backbone stiffness was one of the significant factors which caused the formation of distinct morphologies for the polyelectrolyte BBPs in contact with surfactants having opposite charges [88].

Nam *et al.* investigated the factors controlling the self-assembled structures of Janus core–shell BBPs [104]. They employed DPD simulations to study the BBPs consisting of polystyrene as the cores and polylactide and poly(n-butyl acrylate) as the shells. It was shown that the curvature of the BBPs and the stiffness of the backbones were leading factors determining the morphology of the assembled structure. Polylactide was positioned in the outer layer of the self-assembled structure because the solvent was slightly more favorable to Polylactide. Accordingly, it was revealed that increasing the backbone bending energy by shifting the backbone toward polystyrene/poly(n-butyl acrylate) interface and elongating the backbone length contributed to the formation of a less curved structure. As a result, the self-assembled structure was more likely to form a monolayer vesicle rather than the formation of micelles [104]. Experimental and theoretical investigation by Sunday *et al.* revealed that triblock polymers could exhibit atypical phase behavior due to an unexpected flexibility [44]. Employing SCFT, they indicated that although triblock BBPs had a tendency to have a stretched backbone because of the steric hindrance of the densely grafted chains, they represented a loop conformation in a thin film. Consequently, it resulted in the formation of lamellar morphology with a layer consisting of the midblock chains at the interface. Hence, the arrangement of the midblock at the air interface was regarded as evidence of the high flexibility of BBPs [44].

6.2. Self-assembled microstructures of BBPs

Lazutin *et al.* employed computational modeling and simulations in order to elucidate the diagram of states resulting from the self-assembly of planar BBPs grafted on a surface [238]. They indicated that BBPs with amphiphilic monomers self-organized into various structures, illustrating four regions including disordered arrangement of monomers, strands consisting of a small number of chains, and lamellae with small and large domain space. Moreover, a transitional region between lamellar zones was observed, which connected the lamellae with small

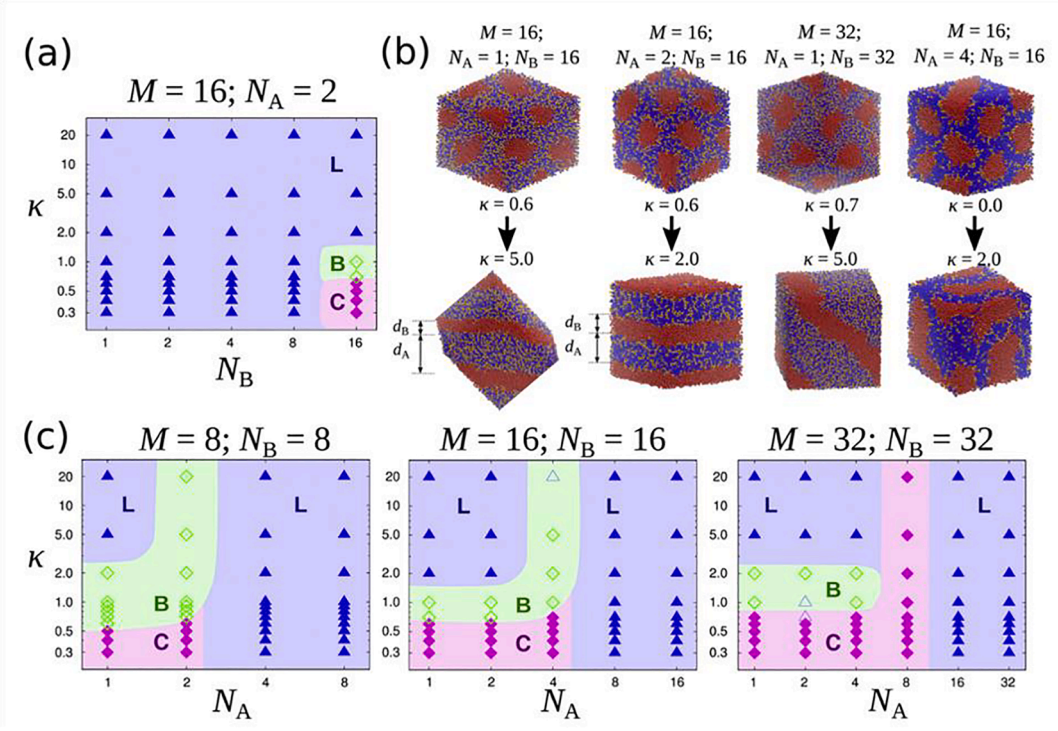

Fig. 8. (a) Morphology diagram for M = 16 of BB diblock copolymers with $N_A = 2$ as function of N_B and k. (b) Snapshots illustrating crossovers from cylinders to lamellar or bicontinuous morphologies for different cases as indicated. (c) Morphology diagrams for M = 8 (left), 16 (center), and 32 (right) of bottlebrush diblock copolymers based on the variation of the backbone stiffness, k, and the length of the A-block side chains ($N_B = M$), B-block side chains $N_B = M$. The symbols correspond to lamellae (triangles), cylinders (fill diamonds), and bicontinuous (open diamonds), and metastable (open triangles). *Reprinted from* [71], *Copyright (2016), with permission from Elsevier.*

and large domain spacings. These connections resembled bridges between locally parallel lamellae [238]. Wessels *et al.* investigated the effect of various architectures of polymers on their self-assembly near/on a solvophobic surface [239]. They used MD simulations to investigate the self-assembly of linear polymers and BBPs with different solvophobic backbone and side chain lengths. They showed that away from the surface, the self-assembly of all structures were similar to that of in bulk. However, near or on the surface, the attraction energy between the surface and polymer had a considerable effect. It was shown that when the strength of attraction between surface and backbone was increased, BBPs with backbones considerably larger than the chains transitioned from a hemispherical domain structure to striped and continuous structures. However, BBPs with backbones notably smaller than the side chains exhibited the largest sensitivity to the energy values and formed different structures. It was also shown that the surface-BBP attraction energy could not noticeably affect BBPs with backbone and side chains with similar lengths [239].

Wang *et al.* investigated the self-assembly of BBPs consisting of hydrophilic backbone and hydrophobic side chains in aqueous solutions using DPD simulations [102]. Their study resulted in well-known self-assembled structures including spherical, cylindrical and lamellar structures (Fig. 9A). Moreover, three other, more complex structures, namely, perforated lamella (PL), cross-linking lamella (CL) and network cylinder (NC) were also observed. PL structure was almost similar to lamellar structure except the perforated pores in lamellae, while CL was constructed by a combination of lamella and cylindrical structures which appeared as cross-linking between two lamellae. NC was completely built with cylindrical BBPs and formed structures resembling a symmetric network. Fig. 9A illustrates self-assembled structures from two views in a three-dimensional space and the relevant density profiles of backbone and side chains. Changing the number of side chain beads (N_S) and backbone beads (N_M) in several BBP concentrations (ρ_B) resulted in creating phase diagrams showing various structural zones [102].

The lamellar periodicity of self-assembled structures, which shows the length of fully extended BBPs in a bilayer lamellar structure, was investigated by Dalsin *et al.* using SCFT and experimental methods [122]. They studied BBPs with polypropylene and polystyrene block side chains and polynorbornene backbones with different contour lengths (L). It was revealed that BBPs self-assembled into lamellar phase and its period (d_0) could be determined by the scaling correlation as $d_0 \propto L^{\gamma}$, where γ could vary from 0.3 to 0.9 at small and large values of L, respectively. This range of exponent implies a structural transition from star-like conformations that are formed for BBPs with similar backbone and side chain lengths to bottlebrush conformation for BBPs with longer backbones compared to side chains. The SCFT results revealed a high desire of backbone to be oriented at the interface of the blocks [122]. Besides, another SCFT study by Levi *et al.* investigated the self-assembly of BBPs with poly(lactide) and poly(4-methyl-ε- caprolactone) side chains [240]. Using the symmetric volume fraction of these side chains, they demonstrated the formation of lamellar structures whose domain spacing was significantly dependent on the backbone length. Kawamoto *et al.* implemented SCFT integrated with an experimental approach to study the self-assembly of Janus-type BBPs. They showed that the phase separation and molecular packing caused the formation of ordered structures including lamellar, hexagonal and also gyroid morphologies. Their simulation results and experimental observations illustrated the dependency of the microdomain period of these structures on the side chain length rather than backbone length [241]. In addition, Cheng *et al.* studied the self-assembly of block bottlebrush copolymers in a thin film [227]. They observed that the self-assembled structures from the densely packed BBPs formed ordered structures with ultra-small period in the scale of a few nanosecond. The domain spacing and orientation of these morphologies was changed by the side chain length, which was attributed to the volume exclusion of the side chains. Indeed, an increase of the side chain length increased the repulsive forces between them and made them more stretched which resulted in changing the domain spacing [227]. Moreover, using experimental approach and SCFT, Chang *et al.* demonstrated that triblock BBPs with low-χ interaction parameters self-assembled to mixed-domain lamellar morphologies. They showed that the domain spacing of these structures declined with increasing total molar mass. Additionally, they introduced a critical

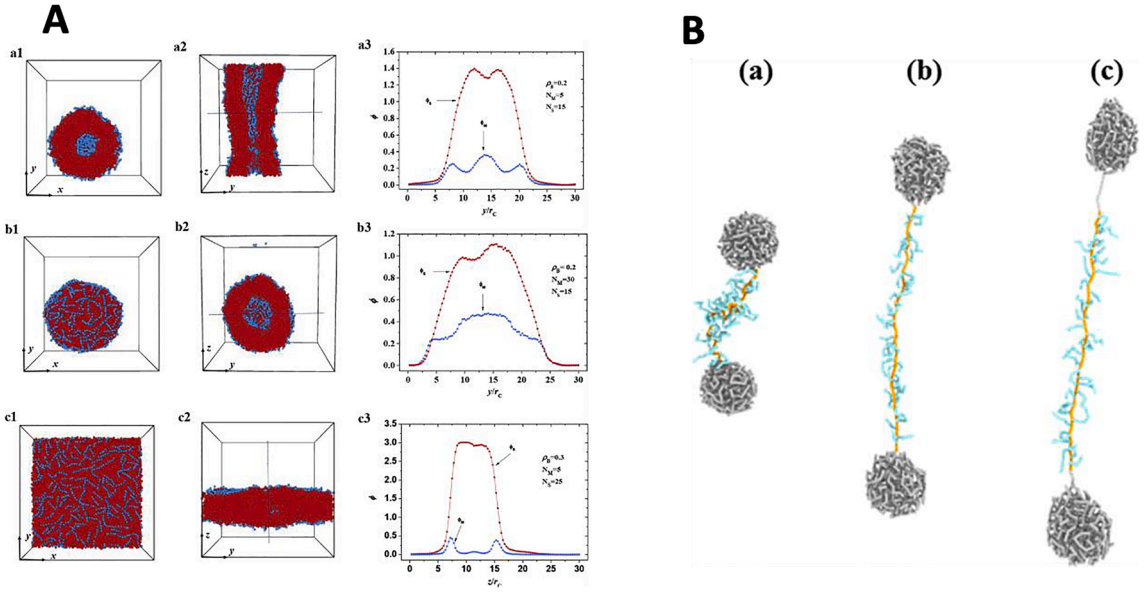

Fig. 9. A) Snapshot for LAM, CYL and SPH microstructures assembled from the bottlebrush molecule, the blue and red colors represent the main and side chains, respectively. The first two columns are bead density distributions for the microstructures without the water molecules from the various views in three-dimensional space, while the last column describes the bead density profiles in one-dimension. (For interpretation of the references to color in this figure legend, the reader is referred to the Web version of this article.) *Reprinted from* [102], *Copyright (2018), with permission from Elsevier.* B) Deformation of a triblock macromolecule in a self-assembled network in elastic deformation (a,b) and yielding (c) regimes. Pictures are snapshots from the molecular dynamic simulations. *Reprinted with permission from* [243] *Copyright (2019) American Chemical Society.* (For interpretation of the references to color in this figure legend, the reader is referred to the web version of this article.)

interaction parameter (χ_{AC}) above which the three-domain lamellar structure was formed [242].

Block BBPs can also be used to form strain-adaptive networks. Liang *et al.* described the deformation behavior of self-assembled structures from triblock polymers consisting of linear-BBP-linear polymer blocks (Fig. 9B) [243]. It was shown that the linear polymers, which were located at the two ends of the bottlebrush backbone, aggregated to form spherical domains. Hence a model specifying mechanical behavior of polymers was offered. This model was validated by MD simulation and experimental data, and it specified two regimes of deformation, depicted in Fig. 9B, as an external force was applied to the self-assembled network. First, the BBP that was bridging between the linear domains stretched out along the backbone and exhibited an elastic deformation. Next, the linear polymers, aggregated at both ends of the BBP were pulled out of their spherical domains to be stretched along the BBP [243].

7. Conclusion and outlook

The capability of BBPs to adopt various conformations and shapes has resulted in distinct structural, mechanical, physical, and rheological properties, which may not be accessible by linear polymers. Their unique structures and self-assembled morphologies have made researchers keen on studying the factors determining the conformations of the side chains and main backbone. As experimental investigation of BBPs can be challenging at the molecular level, different computational and theoretical methods have been successfully employed to study BBPs. It has been shown that the chemical nature of the monomers, the degree of polymerization of the side chains, backbone length and grafting density of side chains can greatly influence BBP structure. In addition, it has been indicated that environmental stimuli such as solvent quality and temperature can affect the structure and properties of these polymer brushes. Herein, we reviewed the computational studies that focus on understanding the effect of these parameters on the conformational specifications and the relevant thermodynamic, physical and mechanical properties as well as their self-assembled structures. These studies including particle-based and field-theory-based simulations can create a context to reveal the evolution of BBP structures under different circumstances like in solvents, on surfaces or in melt states. Moreover, it was observed that changing the architectural parameters of BBPs or their surrounding environment could lead to drastic changes in assembled structures. More importantly, it has been shown that the predictions by these computational methods are in good agreement with experimental approaches.

Even though many of these computational and theoretical studies have provided useful insights that cannot be obtained even with existing advanced characterization methods, computational efficiency can be considered as their main drawback. Due to this, the utility of these methods is limited to certain length- and time-scales. To overcome this, many studies employ certain simplifications in their models to reduce the computational cost, which may result in less accurate predictions. Most studies implicitly simulate the effect of solvent for BBPs in solutions rather than implementing explicit solvent molecules as the implicit solvent approach is computationally efficient. While the use of implicit solvent models solves some problems, it creates several more by being unable to reproduce polymer–solvent interactions and structure of the solvent at the polymer–solvent interface. In addition, a large number of computational studies simulate side chain lengths which are much smaller than the lengths that can be studied using the current experimental procedures, thus making the validation of these results difficult. Using a limited number of BBPs for self-assembly simulations to reduce the computational cost, is another factor that affects the reliability of simulation results. However, with tremendous improvements in computational simulation capabilities through the use of sophisticated algorithms, accurate models and supercomputers, it is now becoming easier to simulate more realistic systems with better efficiency, thus addressing these drawbacks.

A large number of studies have been conducted considering particle-based models of BBP with rigid backbone or side chains [21,155,192]. Since the intrinsic flexibility of polymers is of prime importance in determining the conformations of BBPs, making them rigid can affect simulated predictions of BBP behaviors. Hence, there is a need to develop accurate, transferable models of BBPs that can sufficiently capture the flexibility of both backbone and side chains in the presence and absence of a solvent. Comparison of BBP properties like elasticity in melt state with other branched polymers with different architectures is another potential area to be studied with computational approaches. In this connection, the prediction of BBP behavior for asymmetric distribution of chains or various brush architectures like dumbbell shape architectures can be investigated. In addition, interfacial properties of bottlebrush polyelectrolytes as well as their surface segregation in the presence of linear polymers can be predicted through simulations.

There are novel architectures of BBPs with a wide range of potential applications, which have only been investigated through experimental approaches. BBPs with dendritic side chain end groups, cylindrical bottlebrush polypseudorotaxanes, functionalized branched BBPs, and specific architectures of branched BBPs, like graft-on-graft and star-like structures consisting of multiple arms of BBPs, are a number of these emerging architectures [233,244–246]. Exploration of the conformations and properties of these BBPs by implementing molecular simulations could provide useful insights at a molecular level, which can be used to synthesize more advanced architectures.

The implementation of machine learning approaches integrated with computational and theoretical methods is another important and emerging field that can be employed to understand and/or predict BBP behaviors. For example, enormous amounts of data generated through molecular simulations can be used to train data-driven models into predicting the conformational and mechanical properties of simulated BBPs and their self-assembled architectures. Deep Learning approaches can be employed to study the internal structures of BBPs, which are challenging to achieve through conventional analysis. Computational burden of simulating these complex structures can also be reduced by employing data driven ML/DL based trajectory predicting algorithms as proposed by Sidky *et al.* [247]. The employment of machine learning approaches integrated with simulations can be immensely helpful in order to understand the fundamental relationship between the complex structures and properties of grafted polymers.

8 Data statement

This is a review article and all the figures have been reused from previously published articles. If the readers want to reproduce the figures, we encourage them to ask for the permission from the authors of the original published articles listed in the references section.

Declaration of Competing Interest

The authors declare that they have no known competing financial interests or personal relationships that could have appeared to influence the work reported in this paper.

Acknowledgements

This work was supported by GlycoMIP, a National Science Foundation Materials Innovation Platform funded through Cooperative Agreement DMR-1933525. S.A.D acknowledges the Start-up Funds from Virginia Tech.

References

[1] L.A. Navarro, D.L. French, S. Zauscher, Synthesis of modular brush polymer-protein hybrids using diazotransfer and copper click chemistry, Bioconjug. Chem. 29 (8) (2018) 2594–2605, https://doi.org/10.1021/acs.bioconjchem.8b0030910.1021/acs.bioconjchem.8b00309.s001.

[2] N. Zhang, S. Huber, A. Schulz, R. Luxenhofer, R. Jordan, Cylindrical molecular Brushes of Poly(2-oxazoline)s from 2-Isopropenyl-2-oxazoline, Macromolecules. 42 (6) (2009) 2215–2221, https://doi.org/10.1021/ma802627y.

[3] S. Panyukov, E.B. Zhulina, S.S. Sheiko, G.C. Randall, J. Brock, M. Rubinstein, Tension amplification in molecular brushes in solutions and on substrates, J. Phys. Chem. B. 113 (12) (2009) 3750–3768, https://doi.org/10.1021/jp807671b.

[4] J. Rzayev, Molecular Bottlebrushes: New opportunities in nanomaterials fabrication, ACS Macro Lett. 1 (9) (2012) 1146–1149, https://doi.org/10.1021/mz300402x.

[5] I. Erukhimovich, P.E. Theodorakis, W. Paul, K. Binder, Mesophase formation in two-component cylindrical bottlebrush polymers, J. Chem. Phys. 134 (5) (2011) 054906, https://doi.org/10.1063/1.3537978.

[6] J. Faivre, B.R. Shrestha, G. Xie, M. Olszewski, V. Adibnia, F. Moldovan, A. Montembault, G. Sudre, T. Delair, L. David, K. Matyjaszewski, X. Banquy, Intermolecular Interactions between Bottlebrush Polymers Boost the Protection of Surfaces against Frictional Wear, Chem. Mater. 30 (12) (2018) 4140–4149, https://doi.org/10.1021/acs.chemmater.8b0167610.1021/acs.chemmater.8b01676.s001.

[7] H. Unsal, S. Onbulak, F. Calik, M. Er-Rafik, M. Schmutz, A. Sanyal, J. Rzayev, Interplay between molecular packing, drug loading, and core cross-linking in bottlebrush copolymer micelles, Macromolecules 50 (4) (2017) 1342–1352, https://doi.org/10.1021/acs.macromol.6b0218210.1021/acs.macromol.6b02182.s001.

[8] J. Motoyanagi, T. Ishikawa, M. Minoda, Stimuli-responsive brush-shaped conjugated polymers with pendant well-defined poly(vinyl ether)s, J. Polymer Sci. Part A: Polymer Chem. 54 (20) (2016) 3318–3325, https://doi.org/10.1002/pola.v54.2010.1002/pola.28220.

[9] A.L. Liberman-Martin, C.K. Chu, R.H. Grubbs, Application of Bottlebrush Block Copolymers as Photonic Crystals, Macromol. Rapid Commun. 38 (13) (2017) 1700058, https://doi.org/10.1002/marc.v38.1310.1002/marc.201700058.

[10] S.L. Pesek, Y.-H. Lin, H.Z. Mah, W. Kasper, B. Chen, B.J. Rohde, M.L. Robertson, G.E. Stein, R. Verduzco, Synthesis of bottlebrush copolymers based on poly (dimethylsiloxane) for surface active additives, Polymer 98 (2016) 495–504, https://doi.org/10.1016/j.polymer.2016.01.057.

[11] P. Deshmukh, H. Yoon, S. Cho, S.Y. Yoon, O.V. Zore, T. Kim, I. Chung, S.-K. Ahn, R.M. Kasi, Impact of poly(ε -caprolactone) architecture on the thermomechanical and shape memory properties, J. Polymer Sci. Part A: Polymer Chem. 55 (20) (2017) 3424–3433, https://doi.org/10.1002/pola.v55.2010.1002/pola.28721.

[12] P.E. Theodorakis, N.G. Fytas, Molecular dynamics simulations of bottle-brush polymers with a flexible backbone under theta and good solvent conditions, Am. J. Cond. Matter Phys. 2 (4) (2012) 101–108, https://doi.org/10.5923/j.ajcmp.20120204.05.

[13] P.E. Theodorakis, H.-P. Hsu, W. Paul, K. Binder, Computer simulation of bottle-brush polymers with flexible backbone: good solvent versus theta solvent conditions, J. Chem. Phys. 135 (16) (2011) 164903, https://doi.org/10.1063/1.3656072.

[14] J.-F. Lutz, Thermo-switchable materials prepared using the OEGMA-Platform, Adv. Mater. 23 (19) (2011) 2237–2243, https://doi.org/10.1002/adma.v23.1910.1002/adma.201100597.

[15] O. Azzaroni, A.A. Brown, W.T.S. Huck, UCST wetting transitions of polyzwitterionic brushes driven by self-association, Angew. Chem. Int. Ed Engl. 45 (11) (2006) 1770–1774, https://doi.org/10.1002/(ISSN)1521-377310.1002/anie.v45:1110.1002/anie.200503264.

[16] K.K. Bejagam, S.K. Singh, R. Ahn, S.A. Deshmukh, Unraveling the conformations of backbone and Side Chains in Thermosensitive Bottlebrush Polymers, Macromolecules. 52 (23) (2019) 9398–9408, https://doi.org/10.1021/acs.macromol.9b0102110.1021/acs.macromol.9b01021.s00110.1021/acs.macromol.9b01021.s00210.1021/acs.macromol.9b01021.s003.

[17] N. Cheng, A.A. Brown, O. Azzaroni, W.T.S. Huck, Thickness-dependent properties of polyzwitterionic brushes, Macromolecules 41 (17) (2008) 6317–6321, https://doi.org/10.1021/ma800625y.

[18] H.-i. Lee, J.R. Boyce, A. Nese, S.S. Sheiko, K. Matyjaszewski, pH-induced conformational changes of loosely grafted molecular brushes containing poly (acrylic acid) side chains, Polymer 49 (25) (2008) 5490–5496, https://doi.org/10.1016/j.polymer.2008.10.001.

[19] Y. Xu, S. Bolisetty, M. Drechsler, B. Fang, J. Yuan, M. Ballauff, A.H.E. Müller, pH and salt responsive poly(N, N-dimethylaminoethyl methacrylate) cylindrical brushes and their quaternized derivatives, Polymer. 49 (18) (2008) 3957–3964, https://doi.org/10.1016/j.polymer.2008.06.051.

[20] S.-I. Yamamoto, J. Pietrasik, K. Matyjaszewski, Temperature- and pH-responsive dense copolymer brushes prepared by ATRP, Macromolecules 41 (19) (2008) 7013–7020, https://doi.org/10.1021/ma8011366.

[21] P.E. Theodorakis, W. Paul, K. Binder, Microphase separation in bottlebrush polymers under poor-solvent conditions, Europhys. Lett. 88 (6) (2009) 63002, https://doi.org/10.1209/0295-5075/88/63002.

[22] J.-M. Carrillo, A.V. Dobrynin, Molecular dynamics simulations of grafted layers of bottle-brush polyelectrolytes, Langmuir. 26 (23) (2010) 18374–18381, https://doi.org/10.1021/la103229u.

[23] M. Saariaho, O. Ikkala, I. Szleifer, I. Erukhimovich, G. ten Brinke, On lyotropic behavior of molecular bottle-brushes: A Monte Carlo computer simulation study, J. Chem. Phys. 107 (8) (1997) 3267–3276, https://doi.org/10.1063/1.474677.

[24] J. Bolton, T.S. Bailey, J. Rzayev, Large pore size nanoporous materials from the self-assembly of asymmetric bottlebrush block copolymers, Nano Lett. 11 (3) (2011) 998–1001, https://doi.org/10.1021/nl103747m.

[25] W. Gu, J. Huh, S.W. Hong, B.R. Sveinbjornsson, C. Park, R.H. Grubbs, T. P. Russell, Self-Assembly of Symmetric Brush Diblock Copolymers, ACS Nano. 7 (3) (2013) 2551–2558, https://doi.org/10.1021/nn305867d.

[26] S.W. Hong, W. Gu, J. Huh, B.R. Sveinbjornsson, G. Jeong, R.H. Grubbs, T. P. Russell, On the self-assembly of brush block copolymers in thin films, ACS Nano. 7 (11) (2013) 9684–9692, https://doi.org/10.1021/nn402639g.

[27] D.J. Walsh, S. Dutta, C.E. Sing, D. Guironnet, Eng. Molecular Geometry Bottlebrush Polym. 52 (13) (2019) 4847–4857, https://doi.org/10.1021/acs.macromol.9b0084510.1021/acs.macromol.9b00845.s001.

[28] D. Chatterjee, T.A. Vilgis, Scaling laws of bottle-brush polymers in dilute solutions, Macromolecular Theory Simul. 25 (6) (2016) 518–523, https://doi.org/10.1002/mats.201600074.

[29] H.-P. Hsu, W. Paul, K. Binder, Structure of bottle-brush polymers in solution: A Monte Carlo test of models for the scattering function, J. Chem. Phys. 129 (20) (2008) 204904, https://doi.org/10.1063/1.3025893.

[30] L. Feuz, F.A.M. Leermakers, M. Textor, O. Borisov, Adsorption of molecular brushes with polyelectrolyte backbones onto oppositely charged surfaces: A self-consistent field theory, Langmuir 24 (14) (2008) 7232–7244, https://doi.org/10.1021/la800272v.

[31] D. Xu, M.J. Williamson, R.C. Walker, Chapter 1 - Advancements in Molecular Dynamics Simulations of Biomolecules on Graphical Processing Units, in: R.A. Wheeler (Ed.), Annual Reports in Computational Chemistry, Elsevier, 2010: pp. 2–19. https://doi.org/10.1016/S1574-1400(10)06001-9.

[32] S.Y. Joshi, S.A. Deshmukh, A review of advancements in coarse-grained molecular dynamics simulations, Mol. Simul. (2020) 1–18, https://doi.org/10.1080/08927022.2020.1828583.

[33] Z. Jing, C. Liu, S.Y. Cheng, R. Qi, B.D. Walker, J.-P. Piquemal, P. Ren, Polarizable Force Fields for Biomolecular Simulations: Recent Advances and Applications, Annu. Rev. Biophys. 48 (1) (2019) 371–394, https://doi.org/10.1146/annurev-biophys-070317-033349.

[34] H.-P. Hsu, W. Paul, A fast Monte Carlo algorithm for studying bottle-brush polymers, Comput. Phys. Commun. 182 (10) (2011) 2115–2121, https://doi.org/10.1016/j.cpc.2011.05.005.

[35] Z. Zhang, J.-M. Carrillo, S.-K. Ahn, B. Wu, K. Hong, G.S. Smith, C. Do, Atomistic structure of bottlebrush polymers: Simulations and Neutron Scattering Studies, Macromolecules. 47 (16) (2014) 5808–5814, https://doi.org/10.1021/ma500613c.

[36] S. Dutta, M.A. Wade, D.J. Walsh, D. Guironnet, S.A. Rogers, C.E. Sing, Dilute solution structure of bottlebrush polymers, Soft Matter. 15 (14) (2019) 2928–2941, https://doi.org/10.1039/C9SM00033J.

[37] Y. Rouault, O.V. Borisov, Comb-Branched Polymers: Monte Carlo Simulation and Scaling, Macromolecules. 29 (1996) 2605–2611, https://doi.org/10.1021/ma951126x.

[38] P. Corsi, E. Roma, T. Gasperi, F. Bruni, B. Capone, Exploiting scaling laws for designing polymeric bottle brushes: a theoretical coarse-graining for homopolymeric branched polymers, Phys. Chem. Chem. Phys. 21 (27) (2019) 14873–14878, https://doi.org/10.1039/C9CP01316D.

[39] M. Abbasi, L. Faust, M. Wilhelm, Comb and bottlebrush polymers with superior rheological and mechanical properties, Adv. Mater. 31 (26) (2019) 1806484, https://doi.org/10.1002/adma.v31.2610.1002/adma.201806484.

[40] S.S. Sheiko, B.S. Sumerlin, K. Matyjaszewski, Cylindrical molecular brushes: Synthesis, characterization, and properties, Progr. Polymer Sci. 33 (7) (2008) 759–785, https://doi.org/10.1016/j.progpolymsci.2008.05.001.

[41] G. Xie, M.R. Martinez, M. Olszewski, S.S. Sheiko, K. Matyjaszewski, Molecular Bottlebrushes as Novel Materials, Biomacromolecules. 20 (1) (2019) 27–54, https://doi.org/10.1021/acs.biomac.8b01171.

[42] J.A. Buckwalter, K.E. Kuettner, E.-M. Thonar, Age-related changes in articular cartilage proteoglycans: electron microscopic studies, J. Orthop. Res. 3 (3) (1985) 251–257, https://doi.org/10.1002/(ISSN)1554-527X10.1002/jor.v3:310.1002/jor.1100030301.

[43] Y. Chen, X. Zhang, Y. Jiang, The influence of side-chain conformations on the phase behavior of bottlebrush block polymers, Soft Matter. 16 (34) (2020) 8047–8056, https://doi.org/10.1039/D0SM00918K.

[44] D.F. Sunday, A.B. Chang, C.D. Liman, E. Gann, D.M. Delongchamp, L. Thomsen, M.W. Matsen, R.H. Grubbs, C.L. Soles, Self-Assembly of ABC Bottlebrush Triblock Terpolymers with Evidence for Looped Backbone Conformations, Macromolecules. 51 (2018). https://www.ncbi.nlm.nih.gov/pubmed/33033416.

[45] A. Aguado, P.A. Madden, Ewald summation of electrostatic multipole interactions up to the quadrupolar level, J. Chem. Phys. 119 (14) (2003) 7471–7483, https://doi.org/10.1063/1.1605941.

[46] O.N. Osychenko, G.E. Astrakharchik, J. Boronat, Ewald method for polytropic potentials in arbitrary dimensionality, Mole. Phys. 110 (4) (2012) 227–247, https://doi.org/10.1080/00268976.2011.640291.

[47] B.A. Wells, A.L. Chaffee, Ewald Summation for Molecular Simulations, J. Chem. Theory Comput. 11 (8) (2015) 3684–3695, https://doi.org/10.1021/acs.jctc.5b00093.

[48] S. Yip, Handbook of Materials Modeling, Springer Science & Business Media, 2007. https://play.google.com/store/books/details?id=0sJaJ5juL9EC.

[49] R.K.W. Spencer, M.W. Matsen, Field-theoretic simulations of bottlebrush copolymers, J. Chem. Phys. 149 (18) (2018) 184901, https://doi.org/10.1063/1.5051744.

[50] G. Fredrickson, The Equilibrium Theory of Inhomogeneous Polymers (2005), https://doi.org/10.1093/acprof:oso/9780198567295.001.0001.

[51] L. Feuz, F.A.M. Leermakers, M. Textor, O. Borisov, Bending rigidity and induced persistence length of molecular bottle brushes: A Self-Consistent-Field Theory, Macromolecules. 38 (2005) 8891–8901, https://doi.org/10.1021/ma050871z.

[52] G.H. Fredrickson, V. Ganesan, F. Drolet, Field-theoretic computer simulation methods for polymers and complex fluids, Macromolecules 35 (1) (2002) 16–39, https://doi.org/10.1021/ma011515t.

[53] Y.O. Popov, J. Lee, G.H. Fredrickson, Field-theoretic simulations of polyelectrolyte complexation, J. Polym. Sci. B Polym. Phys. 45 (24) (2007) 3223–3230, https://doi.org/10.1002/(ISSN)1099-048810.1002/polb.v45:2410.1002/polb.21334.

[54] M.W. Matsen, Field theoretic approach for block polymer melts: SCFT and FTS, J. Chem. Phys. 152 (11) (2020) 110901, https://doi.org/10.1063/1.5145098.

[55] M. Karplus, J. Andrew McCammon, Molecular dynamics simulations of biomolecules, Nature Struct. Biol. 9 (2002) 646–652, https://doi.org/10.1038/nsb0902-646.

[56] P. Procacci, T. Darden, M. Marchi, A very fast molecular dynamics method to simulate biomolecular systems with realistic electrostatic interactions, J. Phys. Chem. 100 (24) (1996) 10464–10468, https://doi.org/10.1021/jp960295w.

[57] Y. Sixto-López, M. Bello, J. Correa-Basurto, Insights into structural features of HDAC1 and its selectivity inhibition elucidated by Molecular dynamic simulation and Molecular Docking, J. Biomol. Struct. Dyn. 37 (3) (2019) 584–610, https://doi.org/10.1080/07391102.2018.1441072.

[58] F. Yan, X. Liu, S. Zhang, J. Su, Q. Zhang, J. Chen, Electrostatic interaction-mediated conformational changes of adipocyte fatty acid binding protein probed by molecular dynamics simulation, J. Biomol. Struct. Dyn. 37 (14) (2019) 3583–3595, https://doi.org/10.1080/07391102.2018.1520648.

[59] M. Murat, G.S. Grest, K. Kremer, Statics and dynamics of symmetric diblock copolymers: A molecular dynamics study, Macromolecules 32 (1999) 595–609, https://doi.org/10.1021/ma981512p.

[60] J.T. Padding, W.J. Briels, Coarse-grained molecular dynamics simulations of polymer melts in transient and steady shear flow, J. Chem. Phys. 118 (22) (2003) 10276–10286, https://doi.org/10.1063/1.1572459.

[61] G. Srinivas, D.E. Discher, M.L. Klein, Self-assembly and properties of diblock copolymers by coarse-grain molecular dynamics, Nat. Mater. 3 (9) (2004) 638–644, https://doi.org/10.1038/nmat1185.

[62] A.N. Rissanou, V. Harmandaris, Structure and dynamics of poly(methyl methacrylate)/graphene systems through atomistic molecular dynamics simulations, J. Nanoparticle Res. 15 (5) (2013), https://doi.org/10.1007/s11051-013-1589-2.

[63] S.Y. Joshi, S. Singh, K.K. Bejagam, S.A. Deshmukh, Dehydration of polymer chains initiates graphene folding in water, Carbon. 180 (2021) 244–253, https://doi.org/10.1016/j.carbon.2021.05.009.

[64] Y. An, S.A. Deshmukh, Machine learning approach for accurate backmapping of coarse-grained models to all-atom models, Chem. Commun. 56 (65) (2020) 9312–9315, https://doi.org/10.1039/D0CC02651D.

[65] Y. An, K.K. Bejagam, S.A. Deshmukh, Development of Transferable Nonbonded Interactions between Coarse-Grained Hydrocarbon and Water Models, J. Phys. Chem. B. 123 (4) (2019) 909–921, https://doi.org/10.1021/acs.jpcb.8b0799010.1021/acs.jpcb.8b07990.s001.

[66] Understanding Molecular Simulation: From Algorithms to Applications, (n.d.). https://books.google.com/books/about/Understanding_Molecular_Simulation.html?id=5qTzldS9ROIC (accessed September 2, 2020).

[67] Computer Simulation of Liquids, (n.d.). https://books.google.com/books/about/Computer_Simulation_of_Liquids.html?id=WFExDwAAQBAJ (accessed September 2, 2020).

[68] D.C. Rapaport, D.C.R. Rapaport, The Art of Molecular Dynamics Simulation, Cambridge University Press, 2004 https://books.google.com/books/about/The_Art_of_Molecular_Dynamics_Simulation.html?hl=&id=iqDJ2hjqBMEC.

[69] A. Chremos, J.F. Douglas, A comparative study of thermodynamic, conformational, and structural properties of bottlebrush with star and ring polymer melts, J. Chem. Phys. 149 (4) (2018) 044904, https://doi.org/10.1063/1.5034794.

[70] D. Chang, M. Lorenz, M.J. Burch, O.S. Ovchinnikova, K. Hong, B.G. Sumpter, J.-M. Carrillo, Structures of Partially Fluorinated Bottlebrush Polymers in Thin Films, ACS Appl. Polymer Mater. 2 (2) (2020) 209–219, https://doi.org/10.1021/acsapm.9b0076310.1021/acsapm.9b00763.s001.

[71] A. Chremos, P.E. Theodorakis, Impact of intrinsic backbone chain stiffness on the morphologies of bottle-brush diblock copolymers, Polymer. 97 (2016) 191–195, https://doi.org/10.1016/j.polymer.2016.05.034.

[72] Q.H. Zeng, A.B. Yu, G.Q. Lu, Multiscale modeling and simulation of polymer nanocomposites, Progr. Polymer Sci. 33 (2) (2008) 191–269, https://doi.org/10.1016/j.progpolymsci.2007.09.002.

[73] S.C. Glotzer, W. Paul, Molecular and mesoscale simulation methods for polymer materials, Ann. Rev. Mater. Res. 32 (1) (2002) 401–436, https://doi.org/10.1146/annurev.matsci.32.010802.112213.

[74] F.K. von Gottberg, F.K. von Gottberg, K.A. Smith, T, Alan Hatton, Stochastic dynamics simulation of surfactant self-assembly, J. Chem. Phys. 106 (1997) 9850–9857, https://doi.org/10.1063/1.473873.

[75] Q. Zhang, J. Lin, L. Wang, Z. Xu, Theoretical modeling and simulations of self-assembly of copolymers in solution, Progr. Polym. Sci. 75 (2017) 1–30, https://doi.org/10.1016/j.progpolymsci.2017.04.003.

[76] A. Jain, P. Sunthar, B. Dünweg, J.R. Prakash, Optimization of a Brownian-dynamics algorithm for semidilute polymer solutions, Phys. Rev. E Stat. Nonlin. Soft Matter Phys. 85 (2012), 066703, https://doi.org/10.1103/PhysRevE.85.066703.

[77] T.W. Liu, Flexible polymer chain dynamics and rheological properties in steady flows, J. Chem. Phys. 90 (10) (1989) 5826–5842, https://doi.org/10.1063/1.456389.

[78] W. Zylka, H.C. Öttinger, A comparison between simulations and various approximations for Hookean dumbbells with hydrodynamic interaction, J. Chem. Phys. 90 (1) (1989) 474–480, https://doi.org/10.1063/1.456690.

[79] P.S. Doyle, E.S.G. Shaqfeh, A.P. Gast, Dynamic simulation of freely draining flexible polymers in steady linear flows, J. Fluid Mech. 334 (1997) 251–291, https://doi.org/10.1017/s0022112096004302.

[80] J. Rotne, S Prager, Variational treatment of hydrodynamic interaction in polymers, J. Chem. Phys. 50 (11) (1969) 4831–4837, https://doi.org/10.1063/1.1670977.

[81] H. Yamakawa, Transport properties of polymer chains in dilute solution: Hydrodynamic interaction, J. Chem. Phys. 53 (1) (1970) 436–443, https://doi.org/10.1063/1.1673799.

[82] C.-C. Hsieh, L. Li, R.G. Larson, Modeling hydrodynamic interaction in Brownian dynamics: Simulations of extensional flows of dilute solutions of DNA and polystyrene, J. Nonnewton. Fluid Mech. 113 (2-3) (2003) 147–191, https://doi.org/10.1016/S0377-0257(03)00107-1.

[83] C.M. Schroeder, R.E. Teixeira, E.S.G. Shaqfeh, S. Chu, Dynamics of DNA in the flow-gradient plane of steady shear flow: Observations and simulations, Macromolecules. 38 (2005) 1967–1978, https://doi.org/10.1021/ma0480796.

[84] D.L. Ermak, J.A. McCammon, Brownian dynamics with hydrodynamic interactions, J. Chem. Phys. 69 (4) (1978) 1352–1360, https://doi.org/10.1063/1.436761.

[85] C. Stoltz, J.J. de Pablo, M.D. Graham, Concentration dependence of shear and extensional rheology of polymer solutions: Brownian dynamics simulations, J. Rheol. 50 (2) (2006) 137–167, https://doi.org/10.1122/1.2167468.

[86] P. Grassia, E.J. Hinch, Computer simulations of polymer chain relaxation via Brownian motion, J. Fluid Mech. 308 (1996) 255–288, https://doi.org/10.1017/s0022112096001474.

[87] Hans Christian Öttinger (Ed.), Stochastic Processes in Polymeric Fluids, Springer Berlin Heidelberg, Berlin, Heidelberg, 1996.

[88] Q. Cao, C. Zuo, L. Li, H. He, Self-assembled nanostructures of bottle-brush polyelectrolytes with oppositely charged surfactants: a computational simulation study, Soft Matter. 7 (14) (2011) 6522, https://doi.org/10.1039/c1sm05528c.

[89] S. Dutta, T. Pan, C.E. Sing, Bridging Simulation Length Scales of Bottlebrush Polymers Using a Wormlike Cylinder Model, Macromolecules. 52 (13) (2019) 4858–4874, https://doi.org/10.1021/acs.macromol.9b00363.

[90] P. J Hoogerbrugge, J. M. V. A Koelman, J M V, Simulating Microscopic Hydrodynamic Phenomena with Dissipative Particle Dynamics, Europhys. Lett. (EPL). 19 (3) (1992) 155–160, https://doi.org/10.1209/0295-5075/19/3/001.

[91] R.L.C. Akkermans, W.J. Briels, Coarse-grained dynamics of one chain in a polymer melt, J. Chem. Phys. 113 (15) (2000) 6409–6422, https://doi.org/10.1063/1.1308513.

[92] J.B. Avalos, J. Bonet Avalos, A.D. Mackie, Dynamic and transport properties of dissipative particle dynamics with energy conservation, J. Chem. Phys. 111 (1999) 5267–5276, https://doi.org/10.1063/1.479780.

[93] W. Dzwinel, D.A. Yuen, Matching macroscopic properties of binary fluids to the interactions of dissipative particle dynamics, Int. J. Modern Phys. C. 11 (01) (2000) 1–25, https://doi.org/10.1142/S012918310000002X.

[94] W. Dzwinel, D.A. Yuen, A. Two-Level, Discrete-particle approach for simulating ordered colloidal structures, J. Colloid Interface Sci. 225 (2000) 179–190, https://doi.org/10.1006/jcis.2000.6751.

[95] C.M. Wijmans, B. Smit, R.D. Groot, Phase behavior of monomeric mixtures and polymer solutions with soft interaction potentials, J. Chem. Phys. 114 (17) (2001) 7644–7654, https://doi.org/10.1063/1.1362298.

[96] A.G. Schlijper, P.J. Hoogerbrugge, C.W. Manke, Computer simulation of dilute polymer solutions with the dissipative particle dynamics method, J. Rheol. 39 (3) (1995) 567–579, https://doi.org/10.1122/1.550713.

[97] P.V. Coveney, H.de Silva, A. Gomtsyan, A. Whiting, E.S. Boek, Novel approaches to cross-linking high molecular weight polysaccharides: Application to guar-based hydraulic fracturing fluids, Molecular Simul. 25 (5) (2000) 265–299, https://doi.org/10.1080/08927020008024503.

[98] R.D. Groot, P.B. Warren, Dissipative particle dynamics: Bridging the gap between atomistic and mesoscopic simulation, J. Chem. Phys. 107 (11) (1997) 4423–4435, https://doi.org/10.1063/1.474784.

[99] J.B. Gibson, K. Chen, S. Chynoweth, Simulation of particle adsorption onto a polymer-coated surface using the dissipative particle dynamics method, J. Colloid Interface Sci. 206 (2) (1998) 464–474, https://doi.org/10.1006/jcis.1998.5734.

[100] P. Español, P.B. Warren, Perspective: Dissipative particle dynamics, J. Chem. Phys. 146 (15) (2017) 150901, https://doi.org/10.1063/1.4979514.

[101] J.B. Gibson, K. Chen, S. Chynoweth, The equilibrium of a velocity-verlet type algorithm for dpd with finite time steps, Int. J. Modern Phys. C. 10 (01) (1999) 241–261, https://doi.org/10.1142/S0129183199000176.

[102] Z. Wang, X. Wang, Y. Ji, X. Qiang, L. He, S. Li, Bottlebrush block polymers in solutions: Self-assembled microstructures and interactions with lipid membranes, Polymer. 140 (2018) 304–314, https://doi.org/10.1016/j.polymer.2018.02.053.

[103] B. Gumus, M. Herrera-Alonso, A. Ramírez-Hernández, Kinetically-arrested single-polymer nanostructures from amphiphilic mikto-grafted bottlebrushes in solution: A simulation study, Soft Matter. 16 (21) (2020) 4969–4979, https://doi.org/10.1039/D0SM00771D.

[104] J. Nam, Y. Kim, J.G. Kim, M. Seo, Self-assembly of monolayer vesicles via backbone-shiftable synthesis of janus core-shell bottlebrush polymer, Macromolecules. 52 (24) (2019) 9484–9494, https://doi.org/10.1021/acs.macromol.9b0142910.1021/acs.macromol.9b01429.s001.

[105] H.-Y. Chang, Y.-L. Lin, Y.-J. Sheng, H.-K. Tsao, Structural characteristics and fusion pathways of onion-like multilayered polymersome formed by amphiphilic

comb-like graft copolymers, Macromolecules. 46 (14) (2013) 5644–5656, https://doi.org/10.1021/ma400667n.
[106] C.-Y. Teng, Y.-J. Sheng, H.-K. Tsao, Boundary-induced segregation in nanoscale thin films of athermal polymer blends, Soft Matter. 12 (20) (2016) 4603–4610, https://doi.org/10.1039/C6SM00559D.
[107] A.T. Sose, H.D. Cornell, B.J. Gibbons, A.A. Burris, A.J. Morris, S.A. Deshmukh, Modelling drug adsorption in metal–organic frameworks: the role of solvent, RSC Adv. 11 (28) (2021) 17064–17071, https://doi.org/10.1039/D1RA01746B.
[108] K. Binder Applications of the Monte Carlo Method in Statistical Physics, Springer Science & Business Media 2013 https://play.google.com/store/books/details?id=Mu_uCAAAQBAJ.
[109] K. Binder, Monte Carlo and Molecular Dynamics Simulations in Polymer Science, Oxford University Press on Demand, 1995.
[110] D.P. Landau, K. Binder, A Guide to Monte Carlo Simulations in Statistical Physics, Cambridge University Press, 2014 https://play.google.com/store/books/details?id=56ARBgAAQBAJ.
[111] H.-P. Hsu, W. Paul, K. Binder, Conformational studies of bottle-brush polymers absorbed on a flat solid surface, J. Chem. Phys. 133 (13) (2010) 134902, https://doi.org/10.1063/1.3495478.
[112] E. Wernersson, P. Linse, Spreading and brush formation by end-grafted bottle-brush polymers with adsorbing side chains, Langmuir. 29 (33) (2013) 10455–10462, https://doi.org/10.1021/la4021959.
[113] M. Saariaho, O. Ikkala, G. ten Brinke, Molecular bottle brushes in thin films: An off-lattice Monte Carlo study, J. Chem. Phys. 110 (2) (1999) 1180–1187, https://doi.org/10.1063/1.478159.
[114] H.-P. Hsu, W. Paul, K. Binder, Estimation of persistence lengths of semiflexible polymers: Insight from simulations, ВысокоМолекулярные соединения. 55 (2013) 845–865, https://doi.org/10.7868/s050754751306007x.
[115] S. Rathgeber, T. Pakula, A. Wilk, K. Matyjaszewski, H.-i. Lee, K.L. Beers, Bottle-brush macromolecules in solution: Comparison between results obtained from scattering experiments and computer simulations, Polymer. 47 (20) (2006) 7318–7327, https://doi.org/10.1016/j.polymer.2006.06.010.
[116] S. Elli, G. Raffaini, F. Ganazzoli, E.G. Timoshenko, Y.A. Kuznetsov, Surface adsorption of comb polymers by Monte Carlo simulations, Polymer. 49 (6) (2008) 1716–1724, https://doi.org/10.1016/j.polymer.2008.01.058.
[117] S F Edwards, The statistical mechanics of polymers with excluded volume, Proc. Phys. Soc. London. 85 (4) (1965) 613–624, https://doi.org/10.1088/0370-1328/85/4/301.
[118] M W Matsen, The standard Gaussian model for block copolymer melts, J. Phys. Condens. Matter. 14 (2) (2002) R21–R47, https://doi.org/10.1088/0953-8984/14/2/201.
[119] E. Helfand, Theory of inhomogeneous polymers: Fundamentals of the Gaussian random-walk model, J. Chem. Phys. 62 (3) (1975) 999–1005, https://doi.org/10.1063/1.430517.
[120] E. Helfand, Block copolymer theory. III. Statistical mechanics of the microdomain structure, Macromolecules. 8 (4) (1975) 552–556, https://doi.org/10.1021/ma60046a032.
[121] H. Mei, T.S. Laws, J.P. Mahalik, J. Li, A.H. Mah, T. Terlier, P. Bonnesen, D. Uhrig, R. Kumar, G.E. Stein, R. Verduzco, Entropy and enthalpy mediated segregation of bottlebrush copolymers to interfaces, Macromolecules. 52 (22) (2019) 8910–8922, https://doi.org/10.1021/acs.macromol.9b0180110.1021/acs.macromol.9b01801.s001.
[122] S.J. Dalsin, T.G. Rions-Maehren, M.D. Beam, F.S. Bates, M.A. Hillmyer, M. W. Matsen, Bottlebrush Block Polymers: Quantitative Theory and Experiments, ACS Nano. 9 (12) (2015) 12233–12245, https://doi.org/10.1021/acsnano.5b05473.
[123] V. Ganesan, G.H Fredrickson, Field-theoretic polymer simulations, EPL 55 (6) (2001) 814–820, https://doi.org/10.1209/epl/i2001-00353-8.
[124] E. Panagiotou, K.T. Delaney, G.H. Fredrickson, Theoretical prediction of an isotropic to nematic phase transition in bottlebrush homopolymer melts, J. Chem. Phys. 151 (9) (2019) 094901, https://doi.org/10.1063/1.5114698.
[125] W.F.M. Daniel, J. Burdyńska, M. Vatankhah-Varnoosfaderani, K. Matyjaszewski, J. Paturej, M. Rubinstein, A.V. Dobrynin, S.S. Sheiko, Solvent-free, supersoft and superelastic bottlebrush melts and networks, Nat. Mater. 15 (2) (2016) 183–189, https://doi.org/10.1038/nmat4508.
[126] D. Neugebauer, Y. Zhang, T. Pakula, S.S. Sheiko, K. Matyjaszewski, Densely-Grafted and Double-Grafted PEO Brushes via ATRP A Route to Soft Elastomers, Macromolecules. 36 (18) (2003) 6746–6755, https://doi.org/10.1021/ma0345347.
[127] M. Vatankhah-Varnoosfaderani, W.F.M. Daniel, A.P. Zhushma, Q. Li, B.J. Morgan, K. Matyjaszewski, D.P. Armstrong, R.J. Spontak, A.V. Dobrynin, S.S. Sheiko, Bottlebrush Elastomers: A new platform for freestanding electroactuation, Adv. Mater. 29 (2) (2017) 1604209, https://doi.org/10.1002/adma.v29.210.1002/adma.201604209.
[128] M. Ina, Z. Cao, M. Vatankhah-Varnoosfaderani, M.H. Everhart, W.F.M. Daniel, A. V. Dobrynin, S.S. Sheiko, From Adhesion to Wetting: Contact mechanics at the surfaces of super-soft brush-like elastomers, ACS Macro Lett. 6 (8) (2017) 854–858, https://doi.org/10.1021/acsmacrolett.7b0041910.1021/acsmacrolett.7b00419.s001.
[129] W. Wang, W. Lu, A. Goodwin, H. Wang, P. Yin, N.-G. Kang, K. Hong, J.W. Mays, Recent advances in thermoplastic elastomers from living polymerizations: Macromolecular architectures and supramolecular chemistry, Progr. Polymer Sci. 95 (2019) 1–31, https://doi.org/10.1016/j.progpolymsci.2019.04.002.
[130] M. Vatankhah-Varnosfaderani, A.N. Keith, Y. Cong, H. Liang, M. Rosenthal, M. Sztucki, C. Clair, S. Magonov, D.A. Ivanov, A.V. Dobrynin, S.S. Sheiko, Chameleon-like elastomers with molecularly encoded strain-adaptive stiffening and coloration, Science. 359 (6383) (2018) 1509–1513, https://doi.org/10.1126/science:aar5308.
[131] Z. Cao, J.-M.Y. Carrillo, S.S. Sheiko, A.V. Dobrynin, Computer simulations of bottle brushes: From Melts to Soft Networks, Macromolecules 48 (14) (2015) 5006–5015, https://doi.org/10.1021/acs.macromol.5b00682.
[132] M. Jacobs, H. Liang, B. Pugnet, A.V. Dobrynin, Molecular dynamics simulations of surface and interfacial tension of graft polymer melts, Langmuir. 34 (43) (2018) 12974–12981, https://doi.org/10.1021/acs.langmuir.8b02876.
[133] H. Liang, S.S. Sheiko, A.V. Dobrynin, Supersoft and hyperelastic polymer networks with brushlike strands, Macromolecules. 51 (2) (2018) 638–645, https://doi.org/10.1021/acs.macromol.7b0255510.1021/acs.macromol.7b02555.s001.
[134] H. Liang, Z. Cao, Z. Wang, S.S. Sheiko, A.V. Dobrynin, Combs and Bottlebrushes in a Melt, Macromolecules. 50 (8) (2017) 3430–3437, https://doi.org/10.1021/acs.macromol.7b0036410.1021/acs.macromol.7b00364.s001.
[135] H. Liang, G.S. Grest, A.V. Dobrynin, Brush-like polymers and entanglements: From Linear Chains to Filaments, ACS Macro Letters. 8 (10) (2019) 1328–1333, https://doi.org/10.1021/acsmacrolett.9b0051910.1021/acsmacrolett.9b00519.s001.
[136] J. Paturej, S.S. Sheiko, S. Panyukov, M. Rubinstein, Molecular structure of bottlebrush polymers in melts, Sci Adv. 2 (11) (2016) e1601478, https://doi.org/10.1126/sciadv.1601478.
[137] S.M. Aharoni, E.K. Walsh, Rigid Backbone Polymers. 4. Solution Properties of Two Lyotropic Mesomorphic Poly(isocyanates), Macromolecules. 12 (1979) 271–276. https://doi.org/10.1021/ma60068a021.
[138] Takashi Kato (Ed.), Structure and BondingLiquid Crystalline Functional Assemblies and Their Supramolecular Structures, Springer Berlin Heidelberg, Berlin, Heidelberg, 2008.
[139] C. Robinson, Liquid-crystalline structures in polypeptide solutions, Tetrahedron. 13 (1-3) (1961) 219–234, https://doi.org/10.1016/S0040-4020(01)92215-X.
[140] A. Yethiraj, A Monte Carlo simulation study of branched polymers, J. Chem. Phys. 125 (20) (2006) 204901, https://doi.org/10.1063/1.2374884.
[141] P.E. Theodorakis, N.G. Fytas, A study for the static properties of symmetric linear multiblock copolymers under poor solvent conditions, J. Chem. Phys. 136 (9) (2012) 094902, https://doi.org/10.1063/1.3689303.
[142] M. Weißenhofer, D. Pini, G. Kahl, Ordered structures formed by ultrasoft, aspherical particles, Mole. Phys. 116 (21-22) (2018) 2872–2882, https://doi.org/10.1080/00268976.2018.1503353.
[143] N. Borodinov, A. Belianinov, D. Chang, J.-M. Carrillo, M.J. Burch, Y. Xu, K. Hong, A.V. Ievlev, B.G. Sumpter, O.S. Ovchinnikova, Molecular reorganization in bulk bottlebrush polymers: Direct observation via nanoscale imaging, Nanoscale. 10 (37) (2018) 18001–18009, https://doi.org/10.1039/C8NR05630G.
[144] M. Hu, Y. Xia, G.B. McKenna, J.A. Kornfield, R.H. Grubbs, Linear rheological response of a series of densely branched brush polymers, Macromolecules. 44 (17) (2011) 6935–6943, https://doi.org/10.1021/ma2009673.
[145] Z. Cao, W.F.M. Daniel, M. Vatankhah-Varnosfaderani, S.S. Sheiko, A.V. Dobrynin, Dynamics of Bottlebrush Networks, Macromolecules. 49 (20) (2016) 8009–8017, https://doi.org/10.1021/acs.macromol.6b0135810.1021/acs.macromol.6b01358.s001.
[146] M. Doi, S.F. Edwards, S.F. Edwards, The Theory of Polymer Dynamics, Oxford University Press, 1988 https://books.google.com/books/about/The_Theory_of_Polymer_Dynamics.html?hl=&id=dMzGyWs3GKcC.
[147] C.R. López-Barrón, P. Brant, A.P.R. Eberle, D.J. Crowther, Linear rheology and structure of molecular bottlebrushes with short side chains, J. Rheol. 59 (3) (2015) 865–883, https://doi.org/10.1122/1.4918977.
[148] C.R. López-Barrón, M.E. Shivokhin, Extensional strain hardening in highly entangled molecular bottlebrushes, Phys. Rev. Lett. 122 (2019), 037801, https://doi.org/10.1103/PhysRevLett.122.037801.
[149] H. Liang, Z. Wang, A.V. Dobrynin, Scattering from melts of combs and bottlebrushes: Molecular dynamics simulations and theoretical study, Macromolecules. 52 (15) (2019) 5555–5562, https://doi.org/10.1021/acs.macromol.9b01034.
[150] J.M. Sarapas, T.B. Martin, A. Chremos, J.F. Douglas, K.L. Beers, Bottlebrush polymers in the melt and polyelectrolytes in solution share common structural features, Proc. Natl. Acad. Sci. U. S. A. 117 (10) (2020) 5168–5175, https://doi.org/10.1073/pnas.1916362117.
[151] M. Muthukumar, 50th Anniversary Perspective: A Perspective on Polyelectrolyte Solutions, Macromolecules. 50 (24) (2017) 9528–9560, https://doi.org/10.1021/acs.macromol.7b01929.
[152] B. Xu, C. Feng, J. Hu, P. Shi, G. Gu, L. Wang, X. Huang, Spin-casting polymer brush films for stimuli-responsive and anti-fouling surfaces, ACS Appl. Mater. Interfaces. 8 (10) (2016) 6685–6692, https://doi.org/10.1021/acsami.5b12820.
[153] Y. Su, Z. Zhi, Q. Gao, M. Xie, M. Yu, B. Lei, P. Li, P.X. Ma, Autoclaving-derived surface coating with In Vitro and In Vivo Antimicrobial and Antibiofilm Efficacies, Adv. Healthc. Mater. 6 (6) (2017) 1601173, https://doi.org/10.1002/adhm.v6.610.1002/adhm.201601173.
[154] H.-P. Hsu, W. Paul, K. Binder, Structure of bottle brush polymers on surfaces: Weak versus strong adsorption, J. Phys. Chem. B. 115 (48) (2011) 14116–14126, https://doi.org/10.1021/jp204006z.
[155] E. Flikkema, G. ten Brinke, Influence of rigid side chain attraction on stiffness and conformations of comb copolymer brushes strongly adsorbed on a flat surface, Macromolecular Theory Simul. 11 (2002) 777–784, https://doi.org/10.1002/1521-3919(20020901)11:7<777::aid-mats777>3.0.co;2-a.
[156] M. Saariaho, I. Szleifer, O. Ikkala, G. ten Brinke, Extended conformations of isolated molecular bottle-brushes: Influence of side-chain topology,

Macromolecular Theory Simul. 7 (1998) 211–216, https://doi.org/10.1002/(sici)1521-3919(19980301)7:2<211::aid-mats211>3.0.co;2-a.
[157] P.G. Khalatur, A.R. Khokhlov, S.A. Prokhorova, S.S. Sheiko, M. Möller, P. Reineker, D.G. Shirvanyanz, N. Starovoitova, Unusual conformation of molecular cylindrical brushes strongly adsorbed on a flat solid surface, Eur. Phys. J. E - Soft Matter. 1 (1) (2000) 99–103, https://doi.org/10.1007/s101890050012.
[158] J.C. Moreira, N.R. Demarquette, Influence of temperature, molecular weight, and molecular weight dispersity on the surface tension of PS, PP, and PE. I. Experimental, J. Appl. Polym. Sci. 82 (8) (2001) 1907–1920, https://doi.org/10.1002/(ISSN)1097-462810.1002/app.v82:810.1002/app.2036.
[159] G.T Dee, B.B. Sauer, The molecular weight and temperature dependence of polymer surface tension: Comparison of experiment with interface gradient theory, J. Colloid Interface Sci. 152 (1) (1992) 85–103, https://doi.org/10.1016/0021-9797(92)90010-J.
[160] P. Dziezok, K. Fischer, M. Schmidt, S.S. Sheiko, M. Möller, Cylindrical Molecular Brushes, Angew. Chem. Int. Ed Engl. 36 (24) (1997) 2812–2815, https://doi.org/10.1002/(ISSN)1521-377310.1002/anie.v36:2410.1002/anie.199728121.
[161] S. Ujiie, Y. Yano, Thermotropic and lyotropic behavior of novel amphiphilic liquid crystals having hydrophilic poly(ethyleneimine) units, Chem. Commun. (1) (2000) 79–80, https://doi.org/10.1039/a907765k.
[162] Q. Liang, P. Liu, C. Liu, X. Jian, D. Hong, Y. Li, Synthesis and properties of lyotropic liquid crystalline copolyamides containing phthalazinone moiety and ether linkages, Polymer. 46 (16) (2005) 6258–6265, https://doi.org/10.1016/j.polymer.2005.05.059.
[163] J. Paturej, L. Kuban, A. Milchev, V.G. Rostiashvili, T.A. Vilgis, Thermal degradation of adsorbed bottle-brush macromolecules: When Do Strong Covalent Bonds Break Easily? Macromolecular Symposia. 316 (2012) 112–122, https://doi.org/10.1002/masy.201250615.
[164] J.-M.Y. Carrillo, D. Russano, A.V. Dobrynin, Friction between brush layers of charged and neutral bottle-brush macromolecules. molecular dynamics simulations, Langmuir. 27 (23) (2011) 14599–14608, https://doi.org/10.1021/la203525r.
[165] J.-M.Y. Carrillo, W.M. Brown, A.V. Dobrynin, Explicit solvent simulations of friction between brush layers of charged and neutral bottle-brush macromolecules, Macromolecules. 45 (21) (2012) 8880–8891, https://doi.org/10.1021/ma3015849.
[166] G.M. Leuty, M. Tsige, G.S. Grest, M. Rubinstein, Tension amplification in tethered layers of bottle-brush polymers, Macromolecules. 49 (5) (2016) 1950–1960, https://doi.org/10.1021/acs.macromol.5b02305.
[167] D.G. Walton, P.P. Soo, A.M. Mayes, S.J. Sofia Allgor, J.T. Fujii, L.G. Griffith, J. F. Ankner, H. Kaiser, J. Johansson, G.D. Smith, J.G. Barker, S.K. Satija, Creation of Stable Poly(ethylene oxide) Surfaces on Poly(methyl methacrylate) using blends of branched and linear polymers, Macromolecules. 30 (1997) 6947–6956, https://doi.org/10.1021/ma970698+.
[168] S. Sugimoto, Y. Oda, T. Hirata, R. Matsuyama, H. Matsuno, K. Tanaka, Surface segregation of a branched polymer with hydrophilic poly[2-(2-ethoxy) ethoxyethyl vinyl ether] side chains, Polymer Chem. 8 (3) (2017) 505–510, https://doi.org/10.1039/C6PY01984F.
[169] J. Zhang, M.B. Clark, C. Wu, M. Li, P. Trefonas, P.D. Hustad, Orientation Control in Thin Films of a High-χ block copolymer with a surface active embedded neutral layer, Nano Lett. 16 (1) (2016) 728–735, https://doi.org/10.1021/acs.nanolett.5b04602.
[170] H.S. Wang, A. Khan, Y. Choe, J. Huh, J. Bang, Architectural effects of organic nanoparticles on block copolymer orientation, Macromolecules 50 (13) (2017) 5025–5032, https://doi.org/10.1021/acs.macromol.7b00865.
[171] Q. Wei, K. Tajima, Y. Tong, S. Ye, K. Hashimoto, Surface-segregated monolayers: A new type of ordered monolayer for surface modification of organic semiconductors, J. Am. Chem. Soc. 131 (48) (2009) 17597–17604, https://doi.org/10.1021/ja9057053.
[172] A.H. Mah, T. Laws, W. Li, H. Mei, C.C. Brown, A. Ievlev, R. Kumar, R. Verduzco, G.E. Stein, Entropic and enthalpic effects in thin film blends of homopolymers and bottlebrush polymers, Macromolecules. 52 (4) (2019) 1526–1535, https://doi.org/10.1021/acs.macromol.8b0224210.1021/acs.macromol.8b02242.s001.
[173] H.-P. Hsu, W. Paul, S. Rathgeber, K. Binder, Characteristic length scales and radial monomer density profiles of molecular bottle-brushes: Simulation and Experiment, Macromolecules. 43 (3) (2010) 1592–1601, https://doi.org/10.1021/ma902101n.
[174] S. Dutta, C.E. Sing, Two stretching regimes in the elasticity of bottlebrush polymers, Macromolecules. 53 (16) (2020) 6946–6955, https://doi.org/10.1021/acs.macromol.0c0118410.1021/acs.macromol.0c01184.s001.
[175] E.B. Zhulina, S.S. Sheiko, O.V. Borisov, Solution and melts of barbwire bottlebrushes: Hierarchical structure and scale-dependent elasticity, Macromolecules. 52 (4) (2019) 1671–1684, https://doi.org/10.1021/acs.macromol.8b02358.
[176] M. Jacobs, H. Liang, E. Dashtimoghadam, B.J. Morgan, S.S. Sheiko, A. V. Dobrynin, Nonlinear Elasticity and Swelling of Comb and Bottlebrush, Networks 52 (14) (2019) 5095–5101, https://doi.org/10.1021/acs.macromol.9b0095610.1021/acs.macromol.9b00956.s001.
[177] P. Gutjahr, R. Lipowsky, J. Kierfeld, Persistence length of semiflexible polymers and bending rigidity renormalization, Europhysics Letters (EPL). 76 (6) (2006) 994–1000, https://doi.org/10.1209/epl/i2006-10390-3.
[178] I. Teraoka, Polymer Solutions: An Introduction to Physical Properties, Wiley, 2002 https://play.google.com/store/books/details?id=9DpRAAAAMAAJ.
[179] S. Rathgeber, T. Pakula, A. Wilk, K. Matyjaszewski, K.L. Beers, On the shape of bottle-brush macromolecules: systematic variation of architectural parameters, J. Chem. Phys. 122 (12) (2005) 124904, https://doi.org/10.1063/1.1860531.
[180] Y. Nakamura, T. Norisuye, Backbone stiffness of comb-branched polymers, Polymer J. 33 (11) (2001) 874–878, https://doi.org/10.1295/polymj.33.874.
[181] M. Wintermantel, M. Gerle, K. Fischer, M. Schmidt, I. Wataoka, H. Urakawa, K. Kajiwara, Y. Tsukahara, Molecular Bottlebrushes†, Macromolecules. 29 (3) (1996) 978–983, https://doi.org/10.1021/ma950227s.
[182] A. Subbotin, M. Saariaho, O. Ikkala, G. ten Brinke, Elasticity of comb copolymer cylindrical brushes, Macromolecules. 33 (9) (2000) 3447–3452, https://doi.org/10.1021/ma9910311.
[183] T. Hokajo, K. Terao, Y. Nakamura, T. Norisuye, Solution properties of polymacromonomers consisting of polystyrene v effect of side chain length on chain stiffness, Polymer J. 33 (6) (2001) 481–485, https://doi.org/10.1295/polymj.33.481.
[184] A. Gauger, T. Pakula, Static properties of noninteracting comb polymers in dense and dilute media A Monte Carlo Study, Macromolecules. 28 (1) (1995) 190–196, https://doi.org/10.1021/ma00105a025.
[185] K. Terao, Y. Nakamura, T. Norisuye, Solution properties of polymacromonomers consisting of polystyrene. 2. Chain dimensions and stiffness in cyclohexane and toluene, Macromolecules. 32 (3) (1999) 711–716, https://doi.org/10.1021/ma9816517.
[186] G.H. Fredrickson, Surfactant-induced lyotropic behavior of flexible polymer solutions, Macromolecules. 26 (11) (1993) 2825–2831, https://doi.org/10.1021/ma00063a029.
[187] E.B. Zhulina, T.A. Vilgis, Scaling theory of planar brushes formed by branched polymers, Macromolecules. 28 (4) (1995) 1008–1015, https://doi.org/10.1021/ma00108a031.
[188] R.P. Danner, M.S. High, Handbook of Polymer Solution Thermodynamics, John Wiley & Sons, 2010 https://books.google.com/books/about/Handbook_of_Polymer_Solution_Thermodynam.html?hl=&id=TZJDqNCbr2oC.
[189] J.M. Prausnitz R.N. Lichtenthaler E.G. de Azevedo Molecular Thermodynamics of Fluid-Phase Equilibria, Pearson Education 1998 https://play.google.com/store/books/details?id=VSwc1XUmYpcC.
[190] A.R. Khokhlov, A.N. Semenov, Liquid-crystalline ordering in the solution of long persistent chains, Physica A: Stat. Mech. Appl. 108 (2-3) (1981) 546–556, https://doi.org/10.1016/0378-4371(81)90148-5.
[191] N.G. Fytas, P.E. Theodorakis, Molecular dynamics simulations of single-component bottle-brush polymers with flexible backbones under poor solvent conditions, J. Phys. Condens. Matter. 25 (28) (2013) 285105, https://doi.org/10.1088/0953-8984/25/28/285105.
[192] P.E. Theodorakis, W. Paul, K. Binder, Pearl-necklace structures of molecular brushes with rigid backbone under poor solvent conditions: A simulation study, J. Chem. Phys. 133 (10) (2010) 104901, https://doi.org/10.1063/1.3477981.
[193] S.S. Sheiko, O.V. Borisov, S.A. Prokhorova, M. Möller, Cylindrical molecular brushes under poor solvent conditions: microscopic observation and scaling analysis, Eur. Phys. J. E Soft Matter. 13 (2) (2004) 125–131, https://doi.org/10.1140/epje/e2004-00049-8.
[194] P.E. Theodorakis, W. Paul, K. Binder, Interplay between chain collapse and microphase separation in bottle-brush polymers with two types of side chains, Macromolecules. 43 (11) (2010) 5137–5148, https://doi.org/10.1021/ma100414u.
[195] A. Polotsky, M. Charlaganov, Y. Xu, F.A.M. Leermakers, M. Daoud, A.H.E. Müller, T. Dotera, O. Borisov, Pearl-Necklace Structures in Core−Shell Molecular Brushes: Experiments, Monte Carlo Simulations, and Self-Consistent Field Modeling, Macromolecules. 41 (11) (2008) 4020–4028, https://doi.org/10.1021/ma800125q.
[196] L. Liu, V. Abetz, A.H.E. Müller, J. Cylinders, Macromolecules. 36 (2003) 7894–7898, https://doi.org/10.1021/ma0345551.
[197] P.E. Theodorakis, W. Paul, K. Binder, Analysis of the cluster formation in two-component cylindrical bottle-brush polymers under poor solvent conditions: A simulation study, Eur. Phys. J. E Soft Matter. 34 (2011) 52, https://doi.org/10.1140/epje/i2011-11052-5.
[198] H.-P. Hsu, W. Paul, K. Binder, One- and two-component bottle-brush polymers: simulations compared to theoretical predictions, Macromolecular Theory Simul. 16 (7) (2007) 660–689, https://doi.org/10.1002/(ISSN)1521-391910.1002/mats.v16:710.1002/mats.200700031.
[199] J. de Jong, G. ten Brinke, Conformational aspects and intramolecular phase separation of alternating copolymacromonomers: A Computer Simulation Study, Macromolecular Theory Simul. 13 (4) (2004) 318–327, https://doi.org/10.1002/(ISSN)1521-391910.1002/mats.v13:410.1002/mats.200300052.
[200] D. Wang, M.D. Green, K. Chen, C. Daengngam, Y. Kotsuchibashi, Stimuli-responsive polymers: Design, synthesis, characterization, and applications, Int. J. Polymer Sci. 2016 (2016) 1–2, https://doi.org/10.1155/2016/6480259.
[201] M. Wei, Y. Gao, X. Li, M.J. Serpe, Stimuli-responsive polymers and their applications, Polym. Chem. 8 (1) (2017) 127–143, https://doi.org/10.1039/C6PY01585A.
[202] S.A. Deshmukh, S.K.R.S. Sankaranarayanan, K. Suthar, D.C. Mancini, Role of solvation dynamics and local ordering of water in inducing conformational transitions in poly(N-isopropylacrylamide) oligomers through the LCST, J. Phys. Chem. B. 116 (9) (2012) 2651–2663, https://doi.org/10.1021/jp210788u.
[203] S.A. Deshmukh, Z. Li, G. Kamath, K.J. Suthar, S.K.R.S. Sankaranarayanan, D. C. Mancini, Atomistic insights into solvation dynamics and conformational transformation in thermo-sensitive and non-thermo-sensitive oligomers, Polymer. 54 (1) (2013) 210–222, https://doi.org/10.1016/j.polymer.2012.11.009.
[204] J. Hu, S. Liu, Responsive polymers for detection and sensing applications: Current status and future developments, Macromolecules. 43 (20) (2010) 8315–8330, https://doi.org/10.1021/ma1005815.

[205] A.K. Bajpai, S.K. Shukla, S. Bhanu, S. Kankane, Responsive polymers in controlled drug delivery, Prog. Polym. Sci. 33 (11) (2008) 1088–1118, https://doi.org/10.1016/j.progpolymsci.2008.07.005.
[206] D. Parasuraman, M.J. Serpe, Poly (N-isopropylacrylamide) microgels for organic dye removal from water, ACS Appl. Mater. Interfaces. 3 (7) (2011) 2732–2737, https://doi.org/10.1021/am2005288.
[207] X.-Y. Tu, C. Meng, Y.-F. Wang, L.-W. Ma, B.-Y. Wang, J.-L. He, P.-H. Ni, X.-L. Ji, M.-Z. Liu, H. Wei, Fabrication of thermosensitive cyclic brush copolymer with enhanced therapeutic efficacy for anticancer drug delivery, Macromol. Rapid Commun. 39 (5) (2018) 1700744, https://doi.org/10.1002/marc.v39.510.1002/marc.201700744.
[208] D.M. Henn, J.A. Holmes, E.W. Kent, B. Zhao, Worm-to-sphere shape transition of thermoresponsive linear molecular bottlebrushes in moderately concentrated aqueous solution, J. Phys. Chem. B. 122 (27) (2018) 7015–7025, https://doi.org/10.1021/acs.jpcb.8b0476710.1021/acs.jpcb.8b04767.s001.
[209] X. Li, H. ShamsiJazeyi, S.L. Pesek, A. Agrawal, B. Hammouda, R. Verduzco, Thermoresponsive PNIPAAM bottlebrush polymers with tailored side-chain length and end-group structure, Soft Matter. 10 (2014) 2008–2015, https://doi.org/10.1039/c3sm52614c.
[210] S. Lanzalaco, E. Armelin, Poly(N-isopropylacrylamide) and Copolymers: A Review on Recent Progresses in Biomedical Applications, Gels. 3 (4) (2017) 36, https://doi.org/10.3390/gels3040036.
[211] K.K. Bejagam, Y. An, S. Singh, S.A. Deshmukh, Machine-learning enabled new insights into the coil-to-globule transition of thermosensitive polymers using a coarse-grained model, J. Phys. Chem. Lett. 9 (22) (2018) 6480–6488, https://doi.org/10.1021/acs.jpclett.8b0295610.1021/acs.jpclett.8b02956.s001.
[212] Q. Cao, C. Zuo, L. Li, N. Zhang, Conformational Behavior of Bottle-Brush Polyelectrolytes with Charged and Neutral Side Chains, Macromolecular Theory Simul. 19 (6) (2010) 298–308, https://doi.org/10.1002/mats.200900088.
[213] A. Naji, C. Seidel, R.R. Netz, in: Advances in Polymer ScienceSurface-Initiated Polymerization II, Springer-Verlag, Berlin/Heidelberg, 2006, pp. 149–183.
[214] R. Toomey, M. Tirrell, Functional polymer brushes in aqueous media from self-assembled and surface-initiated polymers, Annu. Rev. Phys. Chem. 59 (1) (2008) 493–517, https://doi.org/10.1146/annurev.physchem.59.032607.093623.
[215] S. Das, M. Banik, G. Chen, S. Sinha, R. Mukherjee, Polyelectrolyte brushes: Theory, modelling, synthesis and applications, Soft Matter. 11 (44) (2015) 8550–8583, https://doi.org/10.1039/C5SM01962A.
[216] C.N Likos, R. Blaak, A. Wynveen, Computer simulations of polyelectrolyte stars and brushes, J. Phys.: Cond. Matter. 20 (49) (2008) 494221, https://doi.org/10.1088/0953-8984/20/49/494221.
[217] Spherical polyelectrolyte brushes, Prog. Polym. Sci. 32 (2007) 1135–1151. https://doi.org/10.1016/j.progpolymsci.2007.05.002.
[218] Jürgen Rühe Matthias Ballauff Markus Biesalski Peter Dziezok Franziska Gröhn Diethelm Johannsmann Nikolay Houbenov Norbert Hugenberg Rupert Konradi Sergiy Minko Michail Motornov Roland R. Netz Manfred Schmidt Christian Seidel Manfred Stamm Tim Stephan Denys Usov Haining Zhang 79 150 10.1007/b11268.
[219] D. Russano, J.-M.Y. Carrillo, A.V. Dobrynin, Interaction between brush layers of bottle-brush polyelectrolytes: molecular dynamics simulations, Langmuir. 27 (17) (2011) 11044–11051, https://doi.org/10.1021/la2018067.
[220] O.V. Borisov, E.B. Zhulina, Conformations of polyelectrolyte molecular brushes: A mean-field theory, J. Chem. Phys. 149 (18) (2018) 184904, https://doi.org/10.1063/1.5051353.
[221] R.M. Adar, T. Markovich, D. Andelman, Bjerrum pairs in ionic solutions: A Poisson-Boltzmann approach, J. Chem. Phys. 146 (19) (2017) 194904, https://doi.org/10.1063/1.4982885.
[222] Q.Q. Cao, C.C. Zuo, L.J. Li, Molecular dynamics simulations of end-grafted centipede-like polymers with stiff charged side chains, Eur. Phys. J. E Soft Matter. 32 (1) (2010) 1–12, https://doi.org/10.1140/epje/i2010-10585-3.
[223] P. Linse, P.M. Claesson, Modeling of bottle-brush polymer adsorption onto mica and silica surfaces: Effect of side-chain length, Macromolecules. 43 (4) (2010) 2076–2083, https://doi.org/10.1021/ma902577m.
[224] A.M. Smith, A.A. Lee, S. Perkin, The electrostatic screening length in concentrated electrolytes increases with concentration, J. Phys. Chem. Lett. 7 (12) (2016) 2157–2163, https://doi.org/10.1021/acs.jpclett.6b0086710.1021/acs.jpclett.6b00867.s001.
[225] H. Washizu, T. Kinjo, H. Yoshida, Structure of polyelectrolyte brushes studied by coarse grain simulations, Friction. 2 (1) (2014) 73–81, https://doi.org/10.1007/s40544-014-0041-7.
[226] M. Alaboalirat, L. Qi, K.J. Arrington, S. Qian, J.K. Keum, H. Mei, K.C. Littrell, B. G. Sumpter, J.-M.Y. Carrillo, R. Verduzco, J.B. Matson, Amphiphilic Bottlebrush Block Copolymers: Analysis of aqueous self-assembly by small-angle neutron scattering and surface tension measurements, Macromolecules. 52 (2) (2019) 465–476, https://doi.org/10.1021/acs.macromol.8b0236610.1021/acs.macromol.8b02366.s001.
[227] L.-C. Cheng, K.R. Gadelrab, K. Kawamoto, K.G. Yager, J.A. Johnson, A. Alexander-Katz, C.A. Ross, Templated Self-Assembly of a PS-Branch-PDMS Bottlebrush Copolymer, Nano Lett. 18 (7) (2018) 4360–4369, https://doi.org/10.1021/acs.nanolett.8b0138910.1021/acs.nanolett.8b01389.s001.
[228] J. Rzayev, Synthesis of polystyrene−polylactide bottlebrush block copolymers and their melt self-assembly into large domain nanostructures, Macromolecules. 42 (6) (2009) 2135–2141, https://doi.org/10.1021/ma802304y.
[229] W. Gu, J. Huh, S.W. Hong, B.R. Sveinbjornsson, C. Park, R.H. Grubbs, T.P. Russell, Correction to self-assembly of symmetric brush diblock copolymers, ACS Nano. 9 (7) (2015) 7729, https://doi.org/10.1021/acsnano.5b03233.
[230] Y. Xia, B.D. Olsen, J.A. Kornfield, R.H. Grubbs, Efficient synthesis of narrowly dispersed brush copolymers and study of their assemblies: The importance of side chain arrangement, J. Am. Chem. Soc. 131 (51) (2009) 18525–18532, https://doi.org/10.1021/ja908379q.
[231] B.R. Sveinbjornsson, R.A. Weitekamp, G.M. Miyake, Y. Xia, H.A. Atwater, R. H. Grubbs, Rapid self-assembly of brush block copolymers to photonic crystals, Proc. Natl. Acad. Sci. 109 (36) (2012) 14332–14336, https://doi.org/10.1073/pnas.1213055109.
[232] G.M. Miyake, V.A. Piunova, R.A. Weitekamp, R.H. Grubbs, Precisely tunable photonic crystals from rapidly self-assembling brush block copolymer blends, Angew. Chem. Int. Ed Engl. 51 (45) (2012) 11246–11248, https://doi.org/10.1002/anie.201205743.
[233] R. Verduzco, X. Li, S.L. Pesek, G.E. Stein, Structure, function, self-assembly, and applications of bottlebrush copolymers, Chem. Soc. Rev. 44 (8) (2015) 2405–2420, https://doi.org/10.1039/C4CS00329B.
[234] S.-k. Ahn, J.-M.Y. Carrillo, J.K. Keum, J. Chen, D. Uhrig, B.S. Lokitz, B. G. Sumpter, S. Michael Kilbey, Nanoporous poly(3-hexylthiophene) thin film structures from self-organization of a tunable molecular bottlebrush scaffold, Nanoscale. 9 (21) (2017) 7071–7080, https://doi.org/10.1039/C7NR00015D.
[235] I. Lyubimov, M.G. Wessels, A. Jayaraman, Molecular Dynamics Simulation and PRISM theory study of assembly in solutions of amphiphilic bottlebrush block copolymers, Macromolecules. 51 (19) (2018) 7586–7599, https://doi.org/10.1021/acs.macromol.8b0153510.1021/acs.macromol.8b01535.s001.
[236] M.G. Wessels, A. Jayaraman, Molecular dynamics simulation study of linear, bottlebrush, and star-like amphiphilic block polymer assembly in solution, Soft Matter. 15 (19) (2019) 3987–3998, https://doi.org/10.1039/C9SM00375D.
[237] A. Chremos, P.E. Theodorakis, Morphologies of bottle-brush block copolymers, ACS Macro Lett. 3 (10) (2014) 1096–1100, https://doi.org/10.1021/mz500580f.
[238] A.A. Lazutin, V.V. Vasilevskaya, A.R. Khokhlov, Self-assembly in densely grafted macromolecules with amphiphilic monomer units: Diagram of states, Soft Matter. 13 (45) (2017) 8525–8533, https://doi.org/10.1039/C7SM01560G.
[239] M.G. Wessels, A. Jayaraman, Self-assembly of amphiphilic polymers of varying architectures near attractive surfaces, Soft Matter. 16 (3) (2020) 623–633, https://doi.org/10.1039/C9SM02104C.
[240] A.E. Levi, J. Lequieu, J.D. Horne, M.W. Bates, J.M. Ren, K.T. Delaney, G. H. Fredrickson, C.M. Bates, Miktoarm Stars via Grafting-Through Copolymerization: Self-Assembly and the Star-to-Bottlebrush Transition, Macromolecules. 52 (4) (2019) 1794–1802, https://doi.org/10.1021/acs.macromol.8b0232110.1021/acs.macromol.8b02321.s001.
[241] K. Kawamoto, M. Zhong, K.R. Gadelrab, L.-C. Cheng, C.A. Ross, A. Alexander-Katz, J.A. Johnson, Graft-through Synthesis and Assembly of Janus Bottlebrush Polymers from A-Branch-B Diblock Macromonomers, J. Am. Chem. Soc. 138 (36) (2016) 11501–11504, https://doi.org/10.1021/jacs.6b0767010.1021/jacs.6b07670.s001.
[242] A.B. Chang, C.M. Bates, B. Lee, C.M. Garland, S.C. Jones, R.K.W. Spencer, M. W. Matsen, R.H. Grubbs, Manipulating the ABCs of self-assembly via low-χ block polymer design, Proc. Natl. Acad. Sci. U. S. A. 114 (25) (2017) 6462–6467, https://doi.org/10.1073/pnas.1701386114.
[243] H. Liang, Z. Wang, A.V. Dobrynin, Strain-adaptive self-assembled networks of linear-bottlebrush-linear copolymers, Macromolecules 52 (22) (2019) 8617–8624, https://doi.org/10.1021/acs.macromol.9b01859.
[244] Y. Shi, W. Zhu, Y. Chen, Synthesis of cylindrical polymer brushes with umbrella-like side chains via a combination of grafting-from and grafting-onto methods, Macromolecules. 46 (6) (2013) 2391–2398, https://doi.org/10.1021/ma4001463.
[245] Q. Fu, J.M. Ren, G.G. Qiao, Synthesis of novel cylindrical bottlebrush polypseudorotaxane via inclusion complexation of high density poly (ε-caprolactone) bottlebrush polymer and α-cyclodextrins, Polym. Chem. 3 (2) (2012) 343–351, https://doi.org/10.1039/C1PY00362C.
[246] A.O. Moughton, T. Sagawa, W.M. Gramlich, M. Seo, T.P. Lodge, M.A. Hillmyer, Synthesis of block polymer miktobrushes, Polym. Chem. 4 (1) (2013) 166–173, https://doi.org/10.1039/C2PY20656K.
[247] H. Sidky, W. Chen, A.L. Ferguson, Molecular latent space simulators, Chem. Sci. 11 (35) (2020) 9459–9467, https://doi.org/10.1039/D0SC03635H.